Enhancing Rheological and Ageing Performance of Asphalt Binders Using Hazelnut Shell Biochar Additives

Camila Martínez-Toledo [1,2], Gonzalo Valdés-Vidal [2,*], Alejandra Calabi-Floody [2], María Eugenia González [3], Antonieta Ruiz [3], Cristian Mignolet [2], Jose Norambuena-Contreras [4], Rafael Villegas [5], Jose L. Concha [6]

[1]Engineering Doctoral Program, University of La Frontera, Temuco 4811230, Chile
[2]Department of Civil Engineering, University of La Frontera, Temuco 4811230, Chile
[3]Department of Chemical Engineering, University of La Frontera, Temuco 4811230, Chile
[4]Advanced Bituminous Materials Laboratory, Department of Civil Engineering, Faculty of Science and Engineering, Swansea University, Bay Campus, SA1 8EN, United Kingdom
[5]Department of Chemical Engineering, University of Costa Rica, Costa Rica
[6]LabMAT, Departamento de Ingeniería Civil y Ambiental, Facultad de Ingeniería, Universidad del Bío-Bío, Concepción, 4051381, Chile

[*]Corresponding author: gonzalo.valdes@ufrontera.cl

Abstract

This study evaluated the effect of biochars derived from European hazelnut shells as modifiers of the antioxidant, physical, and rheological properties of asphalt binders used in road construction. Two biochars (BH) were produced via slow pyrolysis at 300 °C (BH1) and 550 °C (BH2) with a residence time of 1 h, and were incorporated into unaged, short-term aged (RTFO), and long-term aged (PAV) asphalt binders. Phenolic compounds of the BHs were identified by liquid chromatography, while their antioxidant effect on asphalt binders was assessed using spectroscopic analyses. Physical properties (rotational viscosity, penetration, softening point, Fraass breaking point) and rheological properties (rutting parameter G*/sin(δ), Rheological Ageing Index, multiple stress creep recovery (MSCR), fatigue parameter (G*·sin(δ), crossover temperature, and complex modulus |G*|) were measured in all ageing states. The main results revealed that both BH mitigated binder ageing, as evidenced by reductions in ageing indices and oxygenated structures. BH1's antioxidant effect was attributed to its phenolic compounds, whereas BH2's effect was attributed to its porous morphology, which facilitated the adsorption of volatiles. Physically, BH reduced viscosity by up to 16 % after PAV ageing, maintained penetration, and lowered the softening point, although Fraass breaking points increased due to particle stiffening. Rheologically, BH improved rutting resistance by up to 8 % during the early ageing stages. After PAV ageing, it mitigated stiffness gain, preserved viscoelastic behaviour, and reduced |G*| at low temperatures compared with the controls. Overall, recycled hazelnut shell BH enhanced ageing resistance and thermal stability of bituminous binders through distinct mechanisms, offering a potentially viable option to extend the service life of road pavement materials.

Keywords: Hazelnut Shell Biochar; Antioxidant properties; Physical properties; Rheological properties, Asphalt ageing

1. Introduction

Asphalt pavements are the most widely used transportation infrastructure for roads and highways worldwide due to their rapid construction and quick opening to traffic [1], [2]. Furthermore, they provide a smooth and comfortable driving surface with low noise impact and ease of maintenance [3], and their materials can be reused for the construction of new asphalt pavements at the end of their service life [4], [5].

Asphalt binder is a key material in the construction of asphalt pavements, although it constitutes a relatively small proportion of the asphalt mixture, accounting for approximately 5 % by weight (wt%) [3]. However, its natural ageing process has a significant impact on the performance and durability of the pavement [6]. The ageing of asphalt binder is promoted by simultaneous volatilisation of light components and oxidation, altering its chemical composition, and thereby affecting its physical, rheological, and mechanical properties [7]. The

volatilisation of light components takes place when the asphalt binder is exposed to high temperatures (above approximately 150 °C) during the production, transport, and placement of the asphalt mixture, leading to an increase in asphaltene content, which reduces its flowability and increases its viscosity [8], [9]. Oxidation, on the other hand, occurs when the organic constituents of the asphalt binder react with atmospheric oxygen due to exposure to heat or ultraviolet (UV) radiation. This chemical ageing process results in an increase in asphaltene levels and a reduction in the content of resins and aromatics [7]. Consequently, the asphalt binder becomes more brittle and susceptible to cracking, reducing its performance at intermediate and low service temperatures [8], [10], [11].

To mitigate the ageing process and improve the properties of asphalt binders, different types of synthetic base modifiers have been proposed, including nanomaterials such as titanium dioxide (nano-TiO_2) [12], zinc oxide (ZnO) [13], and graphene oxide [14]. In addition, other commercial micro-scale modifiers such as graphite [15], [16] and carbon black have also been used [17], [18]. The addition of these additives has shown improvements in the ageing resistance of asphalt binders and performance properties across a wide range of service temperatures. Nevertheless, in response to the current challenges faced by both society and the asphalt industry [19], [20], research efforts have focused on developing sustainable alternatives aimed at environmental protection and energy efficiency [21-23]. In this context, the utilisation of waste materials for the production of value-added products has gained considerable attention [24-26]. One example is the use of agricultural biomass to produce biofuels through pyrolysis [27]. This is a thermal degradation process that occurs in the solid phase of a biomass or plastic material when heated in an inert atmosphere, and it is considered the most effective method for biofuel production [28], [29]. Among the most notable characteristics of pyrolysis is its lower emission of nitrogen oxides (NO_x) and sulphur oxides (SO_x) compared to combustion [30]. Furthermore, it yields three pyrolytic products: bio-oil, syngas, and biochar, respectively [31]. Particularly, biochar is described as a solid material rich in carbon and phenolic compounds [16], [32], whose physicochemical and morphological properties depend on both the feedstock used and the operational conditions of the pyrolysis process, such as temperature, residence time, and heating rate, among others [33], [34]. This variability makes biochar a versatile material, used in a wide range of applications, including soil fertility enhancement, water pollutant removal, and carbon sequestration [34-37]. Its potential as an asphalt binder modifier has also been investigated. Early studies demonstrated that biochar derived from switchgrass can reduce thermal susceptibility and improve rutting resistance in both the asphalt binder and asphalt mixtures, with effects proportional to the biochar content used [38], [39]. This trend has also been reported in more recent studies employing biochar obtained from straw, wood residues, cherries, and sour cherries [40-43]. However, these studies indicate that the addition of biochar may lead to adverse effects on fatigue resistance, moisture sensitivity, and cracking performance; therefore, limiting its dosage is recommended to avoid impairing these properties [38], [39]. Subsequent investigations presented the first findings regarding the influence of biochar on the ageing resistance of asphalt binder [16], [44]. In these studies, the Rheological Ageing Index (RAI) and the ageing index (Iag) were evaluated following the incorporation of biochar derived from *Mesua ferrea* seed shells and wood residues, respectively. In both cases, the results revealed a progressive reduction in binder ageing parameters as the biochar content increased. Nevertheless, these studies did not examine in depth whether this behaviour was associated with potential antioxidant properties related to the original feedstock or with the physicochemical characteristics of the biochar resulting from the pyrolysis process. Moreover, they did not propose a unified mechanistic interpretation linking these factors to binder performance across different ageing stages. More recently, studies have reported that biochars derived from feedstocks such as straw, wood residues, and pig manure are capable of adsorbing volatile organic compounds from asphalt binder when subjected to high temperatures [45], [46]. This phenomenon has been attributed to physical and chemical adsorption mechanisms promoted by the porous structure and high specific surface area of biochar, which contribute to improvements in binder rheological parameters, such as the complex shear modulus, and to mitigating excessive material stiffening [45]. Despite these advances, the extrapolation of these findings to other lignocellulosic biochars remains limited. Furthermore, there is still a lack of comprehensive evaluation of how these properties influence binder performance at different ageing stages (unaged, short-term aged, and long-term aged), as well as their effects on physical and rheological properties across different service temperatures.

Based on this background, the selection of feedstock for biochar production is of critical importance, particularly when the aim is not only to improve the properties of asphalt binder but also to enhance its resistance to ageing. In this regard, the shell of the European hazelnut (HS) from the species *Corylus avellana L*. emerges as a

promising alternative due to its high antioxidant capacity and bioactive potential, attributed to its rich content of phenolic compounds [47-49]. Moreover, lignin accounts for approximately 40 – 50 wt% of HS, followed by 13 – 32 wt% hemicellulose and 16 – 27 wt% cellulose, which gives it a particularly robust structure [49-51]. In addition, HS is the main residue generated during hazelnut processing, representing between 50 % and 70 % of the total fruit weight, depending on the variety and size [50]. This high proportion poses challenges in terms of waste management and final disposal. Furthermore, according to the most recent data, global HS generation has increased by approximately 50 % over the past decade, exceeding 1.2 million tonnes [52]. Traditionally, HS has been used as biomass for combustion in boilers, despite its potential as a source of high-value chemical compounds [50].

A previous study by the authors [53] optimised the slow pyrolysis parameters for producing hazelnut shell (HS) biochar as an asphalt modifier. The analysis, based on a factorial design with three pyrolysis temperatures (300 °C, 425 °C and 550 °C) and three residence times (1, 2 and 3 hours), aimed to enhance the biochar's antioxidant properties and morphological microstructure for volatile adsorption during binder ageing. The results identified two optimal conditions: 300 °C for 1 h (retaining 40 % of HS antioxidant activity) and 550 °C for 1 h (developing a high specific surface area). Both BHs showed a remarkable capacity for chemical interaction with the asphalt binder, attributed to the presence of functional groups mainly composed of carbon, oxygen, and hydrogen elements. Moreover, these achieve a homogeneous dispersion of their particles within the asphalt matrix.

Based on the existing literature, two mechanisms can be proposed to explain the influence of biochar on asphalt binder ageing and on both the physical and rheological performance. Biochars produced at lower pyrolysis temperatures, such as BH1, are expected to retain a higher fraction of phenolic compounds, which may act as radical scavengers and slow down oxidation-driven ageing reactions. In contrast, biochars produced at higher pyrolysis temperatures, such as BH2, typically exhibit a highly porous structure and large specific surface area, which can promote the physical adsorption of volatile components and light fractions during high-temperature exposure, thereby mitigating hardening associated with volatilisation. The contribution of these mechanisms and their combined effect on binder performance across different ageing states and service temperatures has not been comprehensively studied.

In contrast to previous studies on biochar and asphalt, which primarily focus on reporting general improvements in ageing resistance, the present work proposes two ageing mitigation pathways induced by biochars derived from the same feedstock but produced under contrasting pyrolysis conditions. The use of biochar obtained from hazelnut shell enables the exploitation not only of its high phenolic content (associated with free radical scavenging and the retardation of oxidative processes) but also of its porous structure, which may promote the physical adsorption of volatile components at elevated temperatures. Furthermore, the combined application of chemical characterisation techniques, spectroscopic analysis, and rheological evaluation under unaged, short-term aged, and long-term aged conditions allows a direct relationship to be established between the physicochemical properties of the biochar, the ageing mechanisms, and binder performance. This integrated approach extends current knowledge by providing a novel perspective on the potential to tailor biochar to target specific ageing mechanisms in asphalt binders.

In this context, the present study aims to evaluate the effect of two biochars obtained under optimised pyrolysis operating conditions on the antioxidant, physical, and rheological properties of asphalt binder, considering its unaged, RTFO-aged, and PAV-aged conditions. In this way, the present study not only aims to evaluate the potential use of an alternative modifier to improve asphalt binder performance, but also to promote the valorisation of a widely available agricultural residue with limited current applications, thereby contributing to the development of potentially more sustainable and environmentally responsible solutions for the asphalt industry.

2. Materials and methods

2.1. Materials

The BH employed in this investigation were generated through slow pyrolysis in a fixed-bed reactor fitted with an inert nitrogen (N_2) supply operating at a steady flow rate of 0.001 m^3/min. The pyrolysis process was conducted at a controlled heating rate of 3.6 °C/min until reaching the target temperatures, with solid residence times selected according to the optimisation parameters reported by Martínez-Toledo et al. [53], aimed at enhancing the suitability of HS-derived biochar as an asphalt binder modifier. Temperature was monitored using a K-type (NiCr–Ni) thermocouple connected to a proportional–integral–derivative (PID) controller, ensuring stable thermal conditions throughout the process. Pyrolysis was performed under continuous inert gas flow to facilitate the removal of volatile compounds. After pyrolysis, the biochars were allowed to cool naturally under an inert atmosphere to minimise post-oxidation. Identical reactor configuration, purge conditions, heating rate, and cooling procedures were applied to all samples The two selected BH are shown in Figure 1. BH1 was obtained at a pyrolysis temperature of 300 °C, whereas BH2 was produced at 550 °C, both with a residence time of 1 hour. After pyrolysis, each biochar was ground and sieved to obtain a particle size below 20 µm. Figures 1(a) and 1(b) illustrate the pyrolysis-induced transition in particle size from macroscopic and micromorphological perspectives. Figure 1(c) shows the HS used for the production of BH, in which its structure can be observed at both macroscopic and microscopic scales. Figure 1(d), in turn, presents the FTIR spectra of the HS and the biochars, allowing the effect of pyrolysis temperature (reflected in changes in peak transmittance) on the surface functional groups of these materials to be assessed. The physical characteristics of the particles, together with the production yield of both biochars, are summarised in Table 1.

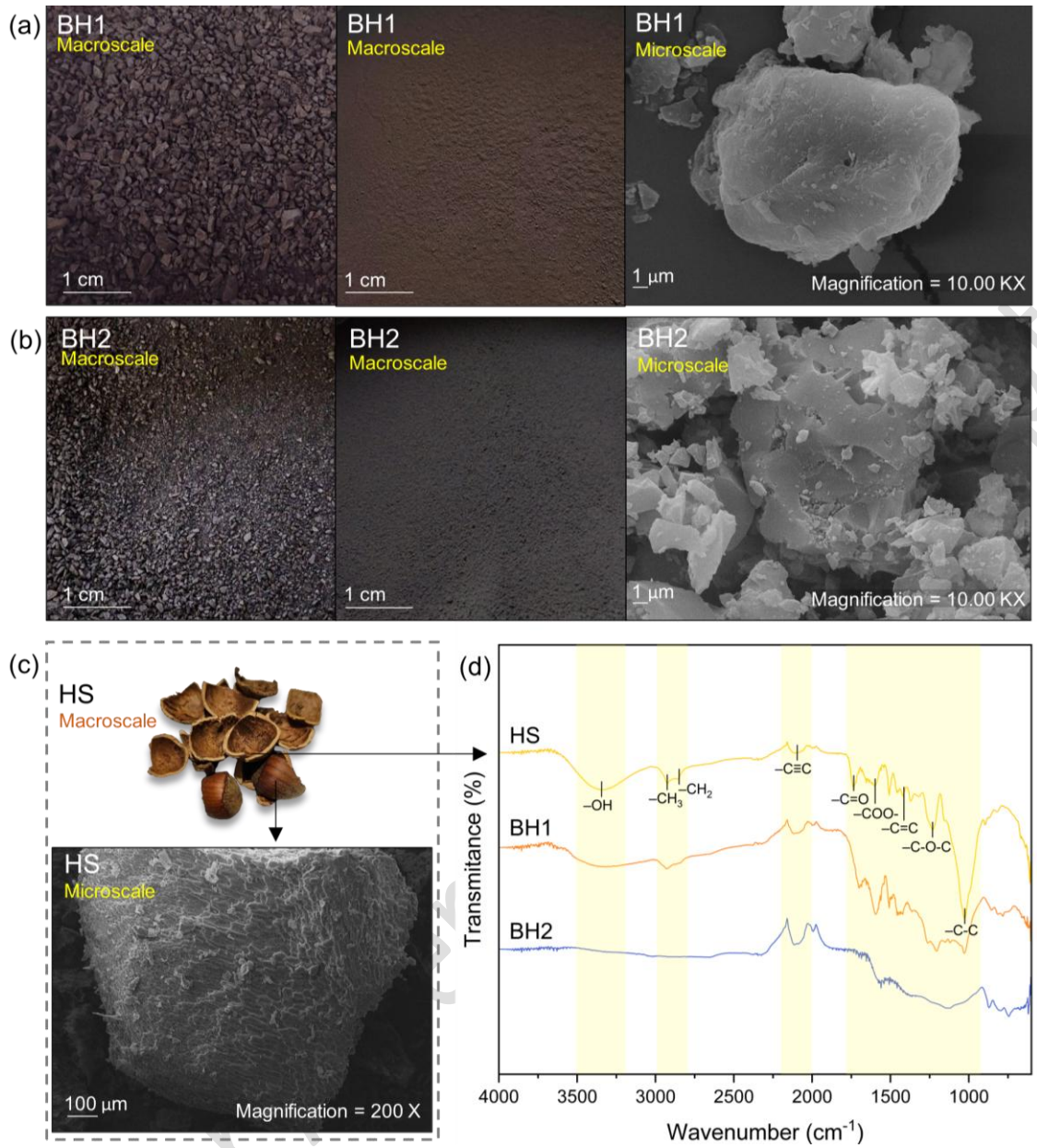

Figure 1. Characteristics of the HS and the biochars used in this study: (a) and (b) show the particle size transition of BH1 and BH2 after pyrolysis, observed at macro and microscale; (c) shows the HS used for the production of BH, in which its structure can be observed at both macroscopic and microscopic scales; (d) shows the FTIR spectra of HS, BH1, and BH2, where the effect of pyrolysis temperature on the surface functional groups of these materials can be observed. Modified from [53].

According to Martínez-Toledo et al. [53], BH1 retains more than 40 % of the antioxidant activity of HS and exhibits the highest production yield (approximately 56 wt%). Conversely, BH2 presents a markedly different chemical composition, with a carbon content of about 84 % (compared with ~ 66 % for BH1) (Table 2), as well as a substantially larger specific surface area of around 290 m^2/g (versus ~ 4.98 m^2/g for BH1), suggesting the formations of a more porous and rougher microstructure upon pyrolysis. Furthermore, both types of BH possess the ability to chemically interact with the asphalt binder through the generation of new functional groups. For BH1, these interactions predominantly involve carbon, oxygen, and hydrogen elements, whereas in BH2 they are mainly carbon-based. In addition, both BH types can be uniformly dispersed within the asphalt binder. In this study, a Performance Grade (PG) 64-22 asphalt binder was employed as both the control material and the base binder for modification with BH.

Table 1. Physical characteristics of the particles, together with the production yield of BH1 and BH2. Modified from [53].

Biochar	**BH1**	**BH2**
Particle size (μm)	<20	<20
Mean particle size (μm)	10.30	9.90
D25	4.52	5.16
D50	10.30	9.90
D75	23.51	18.99
Specific surface area (S_{BET}) (m^2/g)	4.98	290.72
Pore volume (Vp) (cc/g)	0.01	0.02
Pore diameter (Dp) (nm)	3.86	3.27
Production yield of biochar	56 %	32 %

Table 2. Elemental analysis (CHNSO) of the HS, BH1, and BH2. Modified from [53].

Chemical element	**HS**	**BH1**	**BH2**
C	49.37 ± 0.43	66.63 ± 0.64	84.58 ± 1.22
H	7.91 ± 0.41	5.41 ± 0.31	2.96 ± 0.12
N	0.59 ± 0.07	0.59 ± 0.01	0.93 ± 0.03
S	ND	ND	ND
O	42.14 ± 0.49	27.37 ± 0.42	11.54 ± 1.15

Note: ND: Not detected, outside detection limit (1.20 %).

2.2. Modification procedure of the asphalt binder

The modification of the asphalt binder with BH was carried out at 160 ± 5 °C for 30 minutes under mechanical stirring at 350 rpm, as this mixing speed enables a homogeneous dispersion of the biochar particles within the asphalt matrix. In each case, the binder was modified by incorporating 5 wt% biochar (either BH1 or BH2) by total weight of binder. This amount was selected based on previous studies indicating that a biochar content in the range of 2 – 7.5 wt% provides a favourable balance between improved rutting resistance and acceptable fatigue and cracking performance [39], [40], [42], [54]. Subsequently, the samples were maintained at 120 °C for 6 hours to promote coating and adsorption of the asphalt binder onto the BH particles, as recommended in previous studies dealing with biochar–binder interaction mechanisms [43]. This conditioning step was not intended to simulate field ageing, but rather to ensure adequate physicochemical interaction between the solid biochar particles and the asphalt matrix prior to testing.

To quantify and isolate the potential ageing effects associated with the mixing and digestion stage, two control binders were included in the experimental design: “AB” (PG 64-22, unmodified asphalt binder) and “AB+0” (PG 64-22 subjected to the same mixing and digestion protocol, but without the addition of biochar). The inclusion of AB+0 enabled the effects of the mixing and digestion procedure to be distinguished from those specifically induced by the presence of biochar. In addition, two biochar-modified binders were evaluated, namely “AB+BH1” and “AB+BH2”, corresponding to asphalt binders modified with BH1 and BH2, respectively. Figure 2 shows the physicochemical interaction between the binder and the biochars after the modification process. Figure 2(a) presents the chemical interactions as indicated by the FTIR spectra, with peaks corresponding to —C=O and —C–O–C located at 1744 cm^{-1} and 1210 cm^{-1}, respectively. Figures 2(b) and 2(c) illustrate the homogeneous dispersion of BH1 and BH2 particles within the asphalt matrix.

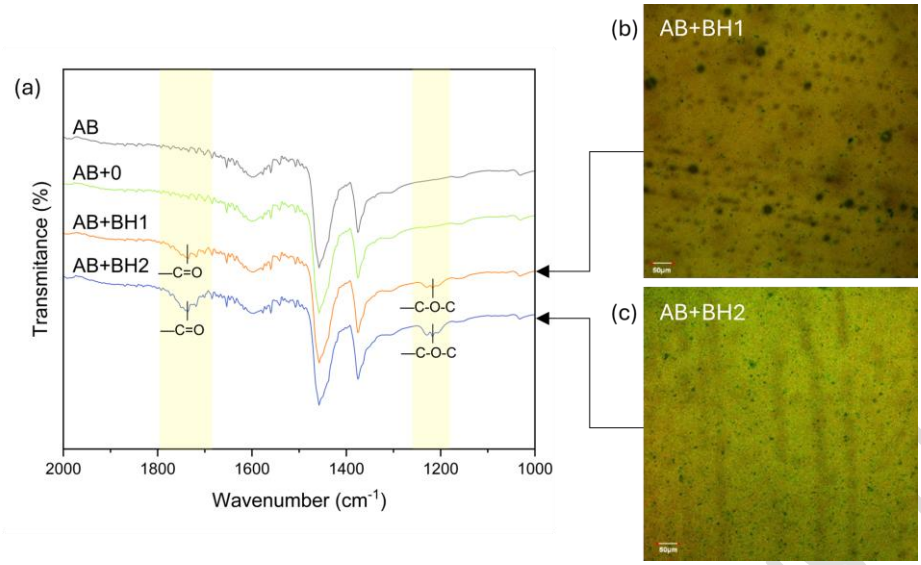

Figure 2. Physicochemical interaction between the binder and the biochars: (a) FTIR spectra of AB, AB+0, AB+BH1, and AB+BH2 showing the peaks corresponding to interactions between the binder and the biochars; (b) and (c) are confocal laser microscopy images of AB+BH1 and AB+BH2, respectively, illustrating the homogeneous dispersion of the biochars within the asphalt matrix. Modified from [53].

2.3. Experimental testing methods

As illustrated in Figure 3, the influence of BH on the physical and rheological properties of the asphalt binder was assessed considering different ageing conditions: unaged, short-term aged (RTFO), and long-term aged (PAV). Short-term ageing was simulated by exposing unaged binder samples to a temperature of 163 °C for 85 minutes in a rolling thin-film oven, in accordance with AASHTO T240 [55]. RTFO mass loss was 0.1 % for the control binders and slightly lower (< 0.1 %) for the biochar-modified binders. Long-term ageing was then reproduced following the procedure described in AASHTO R28 [56], whereby RTFO-aged binders were subjected to a pressure of 2.1 MPa at 100 °C for 20 hours in a pressure ageing vessel.

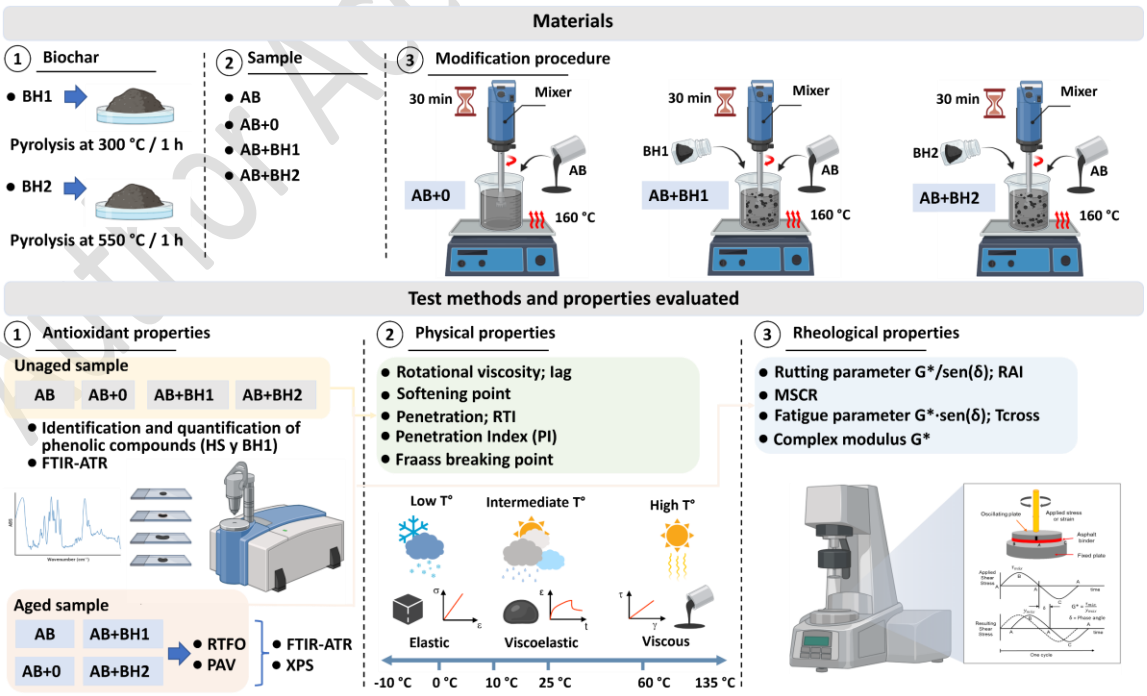

Figure 3. Test methods and evaluated properties.

The following methods were applied to evaluate the properties of HS, BH, and the asphalt binder:

2.3.1. Evaluation of the antioxidant properties

The antioxidant properties of HS and BH were assessed through the identification and quantification of phenolic compounds. The extraction procedure followed the methodology proposed by Nahuelcura et al. [57]. Briefly, 1 g of ground sample was mixed with 3 mL of methanol-formic acid solution (97:3 v/v) and subjected to ultrasonic treatment for 60 seconds at 40 % amplitude, followed by orbital shaking for 10 minutes at 200 × g. The resulting extract was centrifuged at 4000 × g for 15 minutes at 4 °C, filtered through 0.45 μm filters, and stored at -20 °C until analysis.

Phenolic compound identification was carried out using high-performance liquid chromatography coupled with diode array detection (HPLC-DAD) and quadrupole tome-of-flight mass spectrometry (Q-ToF), according to Berrios et al. [58]. Quantification was performed by HPLC-DAD following Nahuelcura et al. [57], using external calibration at 320 nm using 5-caffeoylquinic acid as the reference standard. Antioxidant properties were evaluated using three replicate samples (n = 3).

Chemical alterations resulting from ageing and BH incorporation into the asphalt binder were examined using Fourier-transform infrared spectroscopy equipped with an attenuated total reflectance (FTIR–ATR) accessory. The carbonyl and sulfoxide indices were determined as the ratio of their respective functional group peak areas (A_{1700} for carbonyl, A_{1030} for sulfoxide) to a reference area (Σ_{RA}). Σ_{RA} was defined as the sum of selected peak areas within the 600 – 4000 cm^{-1} wavenumber spectrum, as detailed in Equations (1), (2) and (3), respectively [59]. FTIR–ATR analyses were performed using six replicate spectra per sample (n = 6).

$$\text{Carbonyl index} = \frac{A_{1700}}{\Sigma_{RA}} \quad (1)$$

$$\text{Sulfoxide index} = \frac{A_{1030}}{\Sigma_{RA}} \quad (2)$$

$$\Sigma_{RA} = A_{(2953,\ 2862)} + A_{1700} + A_{1600} + A_{1460} + A_{1376} + A_{1030} + A_{864} + A_{814} + A_{743} + A_{724} \quad (3)$$

Additionally, to provide an overall evaluation of the chemical variations in the asphalt binder induced by the ageing process and the incorporation of BH, a combined ageing index was determined as proposed by Jing et al. [59] and represented in Equation (4).

$$\text{Combined index} = \text{Carbonyl index} + \text{Sulfoxide index} \quad (4)$$

In addition, an antioxidant index was calculated using Equation (5). In this study, this term refers to an FTIR-based indicator derived from changes in oxidation-related indices with respect to the AB+0 binder.

$$\text{Antioxidant index} = \frac{\text{Comb.index}_i - \text{Comb.index}_{AB+0}}{\text{Comb.index}_{AB+0}} \quad (5)$$

where Comb.index_i is the combined index of the AB, AB+BH1 and AB+BH2 samples, respectively, and Comb.index_{AB+0} corresponds to the combined index of the AB+0 sample.

X-ray photoelectron spectroscopy (XPS) was employed to analyse the surface chemical composition of the PAV-aged asphalt binders, with particular emphasis on the oxygen-containing species associated with the O1s region in the biochar-modified samples. Measurements were performed using Al Kα radiation (hν = 1486.6 eV) operated at 15 kV and 20 mA. Survey spectra were acquired over a binding energy range of 0 – 1350 eV with a step size of 1 eV, while high-resolution spectra (O1s) regions were collected with a step size of approximately 0.2 eV. All spectra were charge-corrected by referencing the C1s peak to 284.8 eV. High-resolution spectra

were deconvoluted using a consistent fitting procedure for all samples, employing mixed Gaussian–Lorentzian line shapes and a Shirley background. Based on the XPS data, the O/C ratio was calculated using Equation (6). XPS characterisation was conducted on one representative specimen per binder, with repeated scans used to ensure internal consistency of the measurements.

$$\text{O/C ratio} = \frac{\text{O1s}}{\text{C1s}} \tag{6}$$

Where O1s is the atomic percentage of O1s (%) and C1s is the atomic percentage of C1s (%).

2.3.2. Evaluation of the physical properties of asphalt binder

Rotational viscosity was measured following the procedure outlined in the AASHTO T316–19 standard [60]. Test were conducted at 59 °C, 60 °C and 61 °C for the unaged, RTFO-aged and PAV-aged asphalt binders, respectively, and at 130 °C, 135 °C, 140 °C, 160 °C and 180 °C for the unaged binder. The necessary material was prepared to fill three Brookfield capsules per sample for each condition analysed. The susceptibility to ageing was further evaluated through the ageing index (Iag), determined at 60 °C from the viscosity results. The Iag was calculated according to Equation (7).

$$\text{Iag} = \frac{\text{V}_{\text{aged}}}{\text{V}_{\text{unaged}}} \tag{7}$$

Where V_{aged} is the rotational viscosity of the short-term aged (RTFO) or long-term aged (PAV) asphalt binder, as applicable, in (P), and V_{unaged} is the rotational viscosity of the unaged asphalt binder measured, in (P).

The transition from the viscoelastic to the viscous state was assessed by the softening point, determined in accordance with the ASTM D36–76 standard [61] using the ring-and-ball method.

The hardness of the asphalt binder was evaluated through the penetration test in accordance ASTM D5–13 [62]. A load of 100 g was applied for 5 s at 25 °C. Based on the penetration results, the retained penetration index was calculated using Equation (8).

$$\text{Retained penetration index} = \frac{\text{P}_{\text{aged}}}{\text{P}_{\text{unaged}}} \tag{8}$$

Where P_{aged} is the penetration at 25 °C of the short-term aged (RTFO) or long-term aged (PAV) asphalt binder, as applicable, in (dmm), and P_{unaged} is the penetration at 25 °C of the unaged asphalt binder measured, in (dmm).

Using the softening point results and the penetration measured at 25 °C, the penetration index (PI) was calculated using Equation (9). The PI provides a measure of the thermal susceptibility of asphalt binders to temperature changes, while also offering an indication of their colloidal structure and rheological behaviour [63].

$$\text{PI} = \frac{1952 - 500 \cdot \log(pen) - 20(PA)}{50 \cdot \log(pen) - PA - 120} \tag{9}$$

Where *pen* is the penetration at 25 °C in (dmm) and *PA* is the softening point in (°C).

Finally, the Fraass breaking point was evaluated in accordance with EN 12593:2007 standard [64], to assess the low-temperature behaviour of the asphalt binder [61].

2.3.3. Evaluation of the rheological properties of asphalt binder

Rheological tests were performed using a dynamic shear rheometer (DSR) following the procedure outlined in AASHTO T315 [65]. The rutting resistance was assessed through the rutting parameter G*/sin(δ) at 58 °C, 64 °C, 70 °C and 76 °C. The ageing susceptibility was evaluated using the rheological ageing index (RAI), calculated from G*/sin(δ) results. Lower RAI values indicate reduced ageing susceptibility and, therefore, a binder with greater resistance to ageing-induced damage [66]. The RAI was determined at 64 °C according to Equation (10).

$$\mathrm{RAI} = \frac{(\mathrm{G}^*/\sin(\delta))_{\mathrm{aged}}}{(\mathrm{G}^*/\sin(\delta))_{\mathrm{unaged}}} \quad (10)$$

Where $(G^*/\sin(\delta))_{aged}$ is the rutting parameter of the short-term aged (RTFO) or long-term aged (PAV) asphalt binder, as applicable, expressed in (kPa), and $(G^*/\sin(\delta))_{unaged}$ is the rutting parameter of the unaged asphalt binder, expressed in (kPa).

The MSCR test was performed in accordance with AASHTO T350 [67] to evaluate additional parameters beyond those of the Superpave classification, associated with the load level expected in service [68]. The MSCR test determined the accumulated strain, percentage recovery (*R*), and the non-recoverable creep compliance (*Jnr*) under stress levels of 0.1 and 3.2 kPa. Based on these results, the differential percentage of non-recoverable creep compliance (*Jnr,diff*) and the corresponding traffic level were also obtained. All tests were conducted at 64 °C using RTFO-aged asphalt binders.

Fatigue resistance was evaluated using the rheological parameter G*·sin(δ), according to the procedure described in AASHTO T315 [65], at 16 °C, 19 °C, 22 °C, 25 °C, 28 °C and 31 °C. The crossover temperature (Tcross), at which the storage modulus (G′) equals the loss modulus (G″), was also determined to characterise fatigue performance [69]. PAV-aged samples were tested over a temperature range from 5 °C to 40 °C, with a linear heating rate of 0.5 °C/min, at 1 % strain and an angular frequency of 10 rad/s [70].

Finally, the low-temperature behaviour of the asphalt binder was analysed based on the complex modulus (|G*|), following ASTM D7175–15 [71]. Tests were carried out at -10 °C under 1 % strain and an angular frequency of 10 rad/s [39].

All samples were prepared and analysed in accordance with the protocols specified in their respective standards. Physical and rheological tests were carried out on three independently prepared specimens per binder (n = 3). Prior to statistical analysis, data normality was assessed using the Shapiro–Wilk test, and homogeneity of variances was evaluated using Levene's test. When normality and homoscedasticity assumptions were satisfied, parametric ANOVA followed by appropriate post hoc comparisons was applied. For datasets that did not meet normality assumptions, non-parametric Kruskal–Wallis tests followed by Dunn's post hoc analysis were used. When non-parametric comparisons involved only two independent groups, the Mann–Whitney U test was applied. Statistical significance was evaluated at a confidence level of 95 % (α = 0.05).

3. Results and discussion

3.1. Antioxidant properties

According to the previous findings of Martínez-Toledo et al. [53], the antioxidant activity and total phenolic compounds of HS decrease significantly as both the temperature and residence time of slow pyrolysis increase, reaching values that, in some cases, are considered as traces in BH pyrolysed above 300 °C. Based on these previous findings, the identification and quantification of phenolic compounds were only carried out for HS and BH1 (Table 3). Whereas in BH2, individual phenolic compounds were no detected.

Firstly, HS exhibited a greater number of phenolic compounds than BH1, indicating that pyrolysis leads to the degradation of antioxidant compounds, particularly the more apolar ones, which present a retention time (tR) greater than 18 minutes [72-75]. Among the compounds detected in HS, the material is mainly constituted by those corresponding to peaks 4a, 4b, 7, and 10, of which 3-hydroxy-3-(3-hydroxyphenyl) propanoic acid (4b)

was positively identified. As in other studies of HS [76], some compounds could not be identified; however, their pseudomolecular ions in negative ionisation was detected, as detailed in Table 3.

Table 3. Identification of phenolic compounds in HS and BH1 samples by HPLC-DAD-ESI-MS/MS.

Peak	tR (min)	Compound	λ max (nm)	[M – H]-	Product ion
1	4	Protocatechuic acid	280	153.01	108.00
2a	5	2-hydroxybenzoic acid		137.02	
2b	5	n.i	275	283.04	226.04; 163.02
3	6.5	3,4-dihydroxyphenylacetic acid	310	167.03	152.01
4a	11.5	n.i	280	437.10	
4b	11.5	3-hydroxy-3-(3- hydroxyphenyl) propionic acid		181.04	163.03; 122.03
5	13	Coumarin		147.04	
6	14	n.i	305	195.06	121.02
7	17	n.i		363.10	256.10; 150.00
8a	18	n.i	345	425.09	315.10: 227.10
8b		n.i		377.10	314.10; 149.00
9	18.5	n.i	345	391.10	
10	19	n.i		225.10	166.00; 121.00
11	20.5	Coumaroylquinic acid	350	337.10	
12	26	Isovitexin	345	431.09	284.03

Note: “a”: Compounds identified in HS; “b”: Compounds identified in BH1; Compounds identified both in HS and BH1, excluding “a” and “b”; “tR”: retention time; “[M–H]-”: pseudomolecular ion in negative ionisation mode; “n.i”: no identified.

In BH1, HPLC–DAD quantification showed that some phenolic compounds from HS were retained, particularly those corresponding to peaks 1-7, although in different concentrations (Table 4). Notably, there was a significant increase in 3-hydroxy-3-(3-hydroxyphenyl)propanoic acid (4b) (ANOVA, p-value: < 0.001), whose concentration was up to five times higher than in HS. In addition, phenolic compounds unique to BH1 were also identified, such as 3,4-dihydroxyphenylacetic acid (3) and coumarin (5), which were likely formed during pyrolysis, as they were not detected in HS.

Table 4. Identification of individual phenolic compounds (ug g^{-1}) in HS and BH1 samples by HPLC-DAD, identified according to Table 3.

	HS	BH1	BH2
Peak 1	0.58 ± 0.01	1.93 ± 0.05	n.d
Peak 2	2.59 ± 0.04	6.60 ± 0.07	n.d
Peak 3	n.d	2.08 ± 0.06	n.d
Peak 4	4.81 ± 0.06	24.38 ± 0.16	n.d
Peak 5	n.d	3.32 ± 0.09	n.d
Peak 6	n.d	2.05 ± 0.06	n.d
Peak 7	4.51 ± 0.10	1.14 ± 0.01	n.d
Peak 8	1.19 ± 0.02	n.d	n.d
Peak 9	3.17 ± 0.03	n.d	n.d
Peak 10	3.71 ± 0.07	n.d	n.d
Peak 11	1.38 ± 0.01	n.d	n.d
Peak 12	3.30 ± 0.05	n.d	n.d

Note: “n.d”: no identified.

To evaluate chemical ageing, the evolution of oxidative functional groups in the asphalt binder and the potential antioxidant effect of BH were investigated using FTIR-ATR analysis. Figure 4(a) shows a representative FTIR curve for the tested binders specifying the characteristic peaks and areas for the determination of the carbonyl

and sulfoxide indices. Such indices were selected since they are among the most widely accepted markers of oxidative ageing in bitumen. The authors acknowledge that these indices do not capture other relevant aspects of chemical evolution, such as changes in aromaticity, aliphatic chain distribution, or detailed asphaltene–binder interactions. Although this, they offer a primary analysis on the effect of the BH incorporation into the bituminous material. Since most of the chemical changes associated to binder oxidation are detected in the fingerprint region (< 2000 cm^{-1}), Figure 4(b) shows average FTIR curves for each of the samples in the 600 – 2000 cm^{-1} range. Overall, FTIR analysis shows that both RTFO and PAV ageing induce chemical changes in the virgin binder, evidenced by increased carbonyl (1700 cm^{-1}) and sulfoxide (1030 cm^{-1}) bands. These increases are more pronounced after PAV ageing, reflecting its higher oxidation severity (see AB curves for Unaged, RTFO, and PAV states). The dominant increase in sulfoxides, particularly after PAV ageing, is attributed to the high oxidation reactivity of sulphide compounds in the asphalt binder, as reported by Greenfield et al. [77]. The comparatively smaller increase in the carbonyl index may be related to the lower reactivity of carbonyl-forming species during the oxidative ageing. When comparing the AB and AB+0 curves for each ageing state, it is seen that the mixing process induces a slightly increase in the sulfoxide group being more evident for the PAV-aged state. Regarding the effect of the BH addition, no visual changes are appreciated when comparing the carbonyl and sulfoxide peaks of the AB+0, AB+BH1, and AB+BH2 samples.

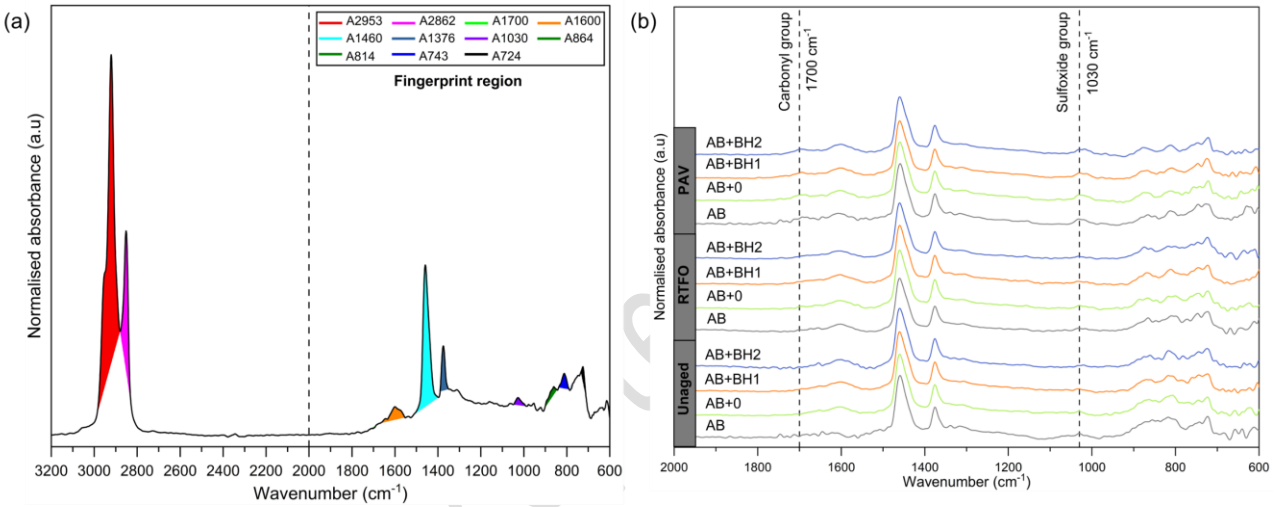

Figure 4. FTIR-ATR spectra of unaged, short-term aged (RTFO), and long-term aged (PAV) asphalt binders used to determine carbonyl and sulfoxide indices: (a) representative spectrum highlighting characteristic peaks and integration regions, and (b) average spectra for each of the binder samples.

To better capture the effect BH addition in the asphalt binders, the Figure 5(a), (b) and (c) present the average results of the carbonyl, sulfoxide, and combined indices, respectively, for the unaged asphalt binder (labelled Un), short-term aged (RTFO), and long-term aged (PAV) samples. A preliminary analysis of Figure 5(a)-(c) indicates that ageing through the RTFO and PAV processes results in an increase in both the carbonyl and sulfoxide indices, reflecting the progressive accumulation of oxygen-containing functional groups due to oxidative degradation. The AB (Un) sample exhibits the lowest values across all three evaluated indices. In contrast, the RTFO and PAV samples show gradual increases, with PAV exhibiting the highest degree of oxidation. These values further increase in AB+0, indicating that the modification process alone accelerates oxidation. The incorporation of BH1 and BH2 into the asphalt binder produces visibly lower oxidation indices at all ageing stages compared to AB+0, suggesting a mitigating effect against oxidative damage. Both BH1 and BH2 demonstrated a similar reduction in the carbonyl index, with BH2 being slightly more effective in decreasing the sulfoxide content, especially in samples aged by RTFO and PAV. From Figure 5(a) and (b), a greater contribution of sulfoxide functional groups to the combined index is evident, which explains the similarity in their trends.

A more detailed analysis of the combined index in Figure 5(c) revealed an increase from approximately 0.0051 in AB (Un) to 0.0146 following RTFO ageing, and up to 0.023 in the PAV-aged sample, representing an overall increase of approximately 57 % compared to the unaged condition. Subsequently, the combined indices for

AB+0 increased further, reaching 0.011 in the unaged sample, 0.017 after RTFO, and 0.0252 following PAV, corresponding to an additional oxidation of approximately 9.6 % to 115 % attributed to the modification process. The greatest variation was observed in AB, indicating that the oxidative contribution of the modification process diminishes with successive RTFO and PAV ageing processes.

The comparison between AB+BH and AB+0 samples demonstrated that the addition of BH markedly reduces the combined index across all ageing states. For instance, the incorporation of BH1 resulted in reductions of 1.9 %, 15.5 %, and 31.15 % in the unaged, RTFO, and PAV samples, respectively. Similarly, BH2 also diminished oxidation, but to a greater extent: 17.4 %, 43.1 %, and 43.3 % for the unaged, RTFO, and PAV samples, respectively. These findings confirm that BH2 exhibits a more pronounced antioxidant effect, particularly in more oxidised asphalt binders. Although BH1 also contributes positively, its efficacy is comparatively lower.

In general, the differences in antioxidant performance between BH1 and BH2 can be attributed to their distinct physicochemical characteristics, influenced by the pyrolysis temperature. In the case of BH1, its higher phenolic content (Table 3) and corresponding antioxidant activity [53] may contribute to free radical scavengers, thereby slowing oxidation reactions during binder ageing, particularly at advanced ageing stages where chemical oxidation is dominant. However, FTIR-based indices should be interpreted as complementary indicators of chemical ageing rather than as a complete representation of the ageing mechanisms involved. Furthermore, elemental analysis of the biochars revealed that BH1 exhibited an average oxygen content of 27.37 %, compared to 11.54 % for BH2 (Table 2). In this context, the higher oxygen content of BH1, together with the oxygen introduced during ageing and modification processes, may contribute to a greater formation of sulfoxides compared to BH2. This observation is therefore proposed as a hypothesis that may partly explain the comparatively higher sulfoxide contribution observed in BH1-modified binders. Conversely, the reduction in oxidation indices observed for BH2 may be associated with its highly porous structure and larger specific surface area, which can promote the physical adsorption of volatile organic compounds during exposure to elevated temperatures [45], [46], [53]. This process may limit volatilisation-related ageing and the subsequent formation of rigid oxidised structures, thereby leading to more effective ageing mitigation at early stages and a reduced degree of long-term hardening. While this interpretation is consistent with the FTIR results, a comprehensive assessment of long-term ageing mitigation requires consideration of additional factors beyond the direct scope of this technique.

To better understand the effect of BH addition on unaged, RTFO-aged, and PAV-aged asphalt binders, Figure 5(d) presents an antioxidant index derived from the combined index of each sample, expressed as a ratio relative to the AB+0 value used as the baseline (with 0 as the reference). The antioxidant index values are shown as positive bars, where a higher value relative to 0 indicates a greater antioxidant effect of the incorporated BH. In all cases, the addition of BH results in positive antioxidant indices, confirming its effectiveness in mitigating oxidative changes. In the unaged asphalt binder, BH1 achieves an antioxidant index of approximately 0.019, compared to 0.17 for BH2. In RTFO-aged samples, BH2 outperforms BH1 with an index of 0.43 versus 0.16, respectively. For PAV-aged samples, BH2 attains an antioxidant index close to 0.43, while BH1 registers a value of 0.31. These results allow us to conclude that BH2 consistently provides a greater antioxidant response at the chemical level, although the difference in this index tends to decrease in PAV-aged asphalt binder. Furthermore, the difference between AB+BH and AB+0 samples suggests that BH addition partially restores the oxidation state of the asphalt binder. In this regard, PAV-aged AB+BH samples approach the oxidation condition of RTFO-aged AB (Figure 5(c)).

Finally, the statistically significant of the differences induced by ageing processes and BH addition on the combined index was evaluated. Based on the obtained p-values (< 0.001), both the individual effects of ageing and BH addition, together with their interaction, resulted in statistically significant differences in the combined index.

Regarding the individual effect of ageing (unaged, RTFO, and PAV), statistically significant differences were observed among all ageing state (p-values: < 0.001). Similarly, with respect to the sample type (AB, AB+0, AB+BH1, and AB+BH2), statistically significant differences were detected (p-values: < 0.001), except between AB and AB+BH1, which exhibited a similar overall effect. More specifically, the simultaneous interactions

revealed that the comparable behaviour for the AB and AB+BH1 samples occurred in the RTFO ageing state. Additionally, comparisons between the AB+BH1 and AB+BH2 samples showed statistically significant differences (p-value: < 0.001) only in the RTFO ageing state. No significant differences were identified between AB+BH1 and AB+BH2 in the unaged (p-value: 0.768) samples or those aged by PAV (p-value: 0.068). These results suggest that BH2 provides a more pronounced oxidation-mitigating effect at the surface level, primarily driven by physical interactions. However, throughout the service life of the pavement, the antioxidant effects of BH1 and BH2 tends to be similar.

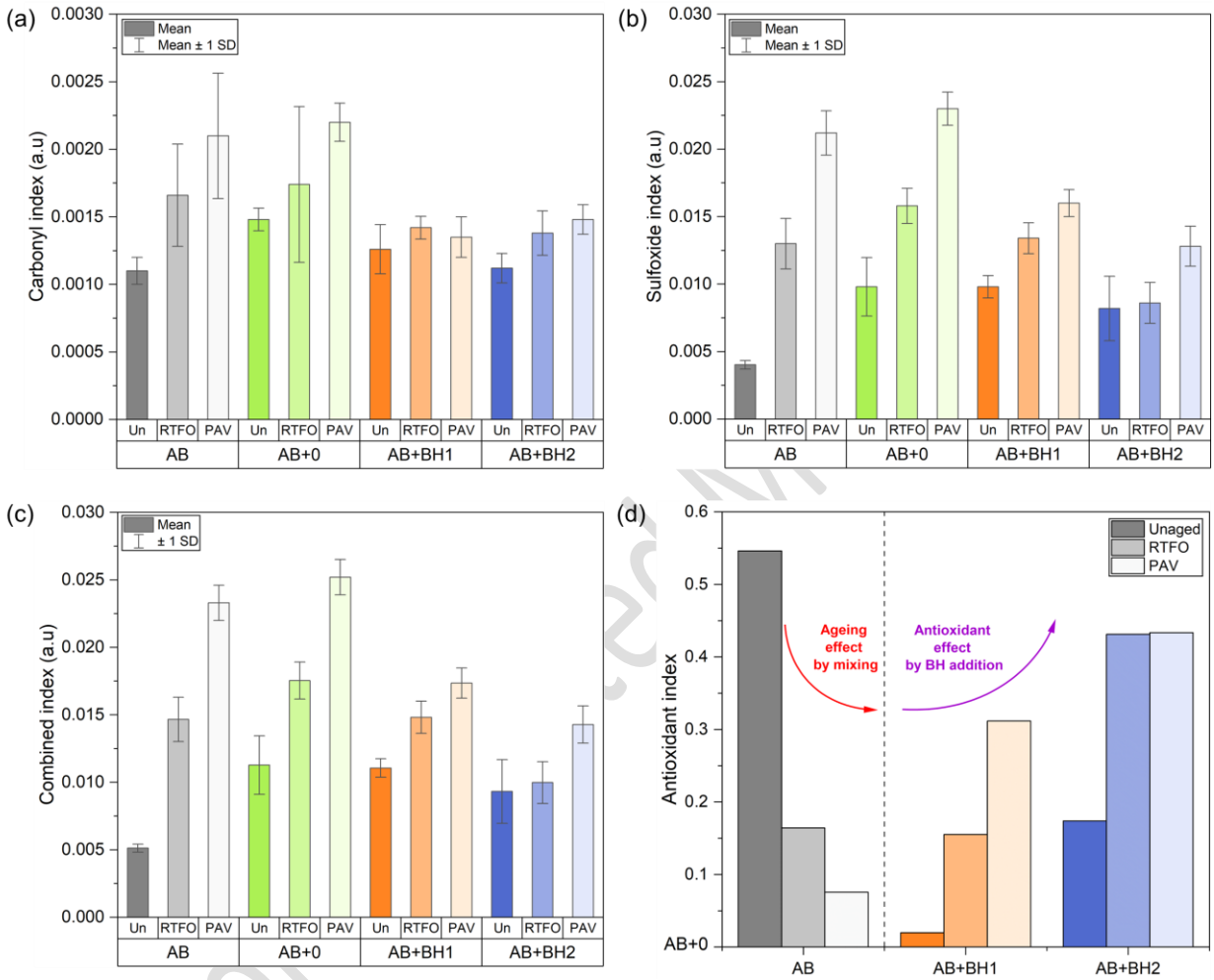

Figure 5. FTIR-ATR-derived indices of asphalt binders: (a) carbonyl; (b) sulfoxide; and (c) combined indices for AB, AB+0, AB+BH1, and AB+BH2 in the unaged (Un), short-term aged (RTFO), and long-term aged (PAV) conditions; (d) antioxidant indices of AB, AB+BH1, and AB+BH2 relative to AB+0.

In order to further investigate the results obtained from the combined index (Figure 5(c)), an XPS analysis was conducted to characterise the chemical changes occurring on the surface of asphalt binders aged by PAV (Figure 6). XPS was employed as a complementary, surface-sensitive technique to provide mechanistic insight into oxidation-related trends. First, the spectral regions corresponding to the O1s and C1s peaks of AB, AB+0, AB+BH1, and AB+BH2 were analysed. Subsequently, a high-resolution study of the O1s peak was performed to identify the individual chemical components present in AB+BH1 and AB+BH2 after PAV ageing.

Figure 6(a) presents the survey spectra for each sample, showing that AB+BH1 and AB+BH2 exhibited lower intensity in the O1s peak compared to AB and AB+0, together with higher intensity in the C1s peak. The latter is primarily attributed to the incorporation of biochar, given its high carbon content (BH1: ~ 67 % carbon; BH2: ~ 85 % carbon) [53]. Given the surface-sensitive and semi-quantitative nature of XPS, the reduced relative O1s signal suggests a lower degree of surface oxygenation in the biochar-modified binders after PAV ageing.

However, this trend reflects the combined influence of ageing-related oxidation processes and the intrinsic elemental composition of the added biochars.

Accordingly, the O/C ratio (Figure 6(b)) must be interpreted with caution, as its reduction in AB+BH1 and AB+BH2 arises from both a decrease in oxygenated species associated with ageing and an increase in carbon contribution from the biochar particles. While the absolute differences in O/C ratio should be regarded as indicative rather than definitive, the consistent decreasing trend, together with the FTIR-derived oxidation indices and rheological ageing parameters, supports the interpretation that the biochar incorporation contributes to the mitigates of oxidation-related ageing effects, particularly at the surface level. In the case of AB+BH1, the O/C ratio decreased by approximately 57 % compared to AB and by 62 % relative to AB+0. For AB+BH2, the reductions were approximately 66 % and 70 %, respectively. Rather than indicating a purely chemical antioxidant effect, the more pronounced decrease observed for BH2 is mainly associated with its highly carbonaceous and porous nature, which may enhance physical interactions and adsorption phenomena at the binder–biochar interface. In this context, the O/C ratio is not considered a direct measure of bulk oxidation, but rather a complementary surface indicator whose relevance is strengthened by its consistency with the FTIR ageing indices.

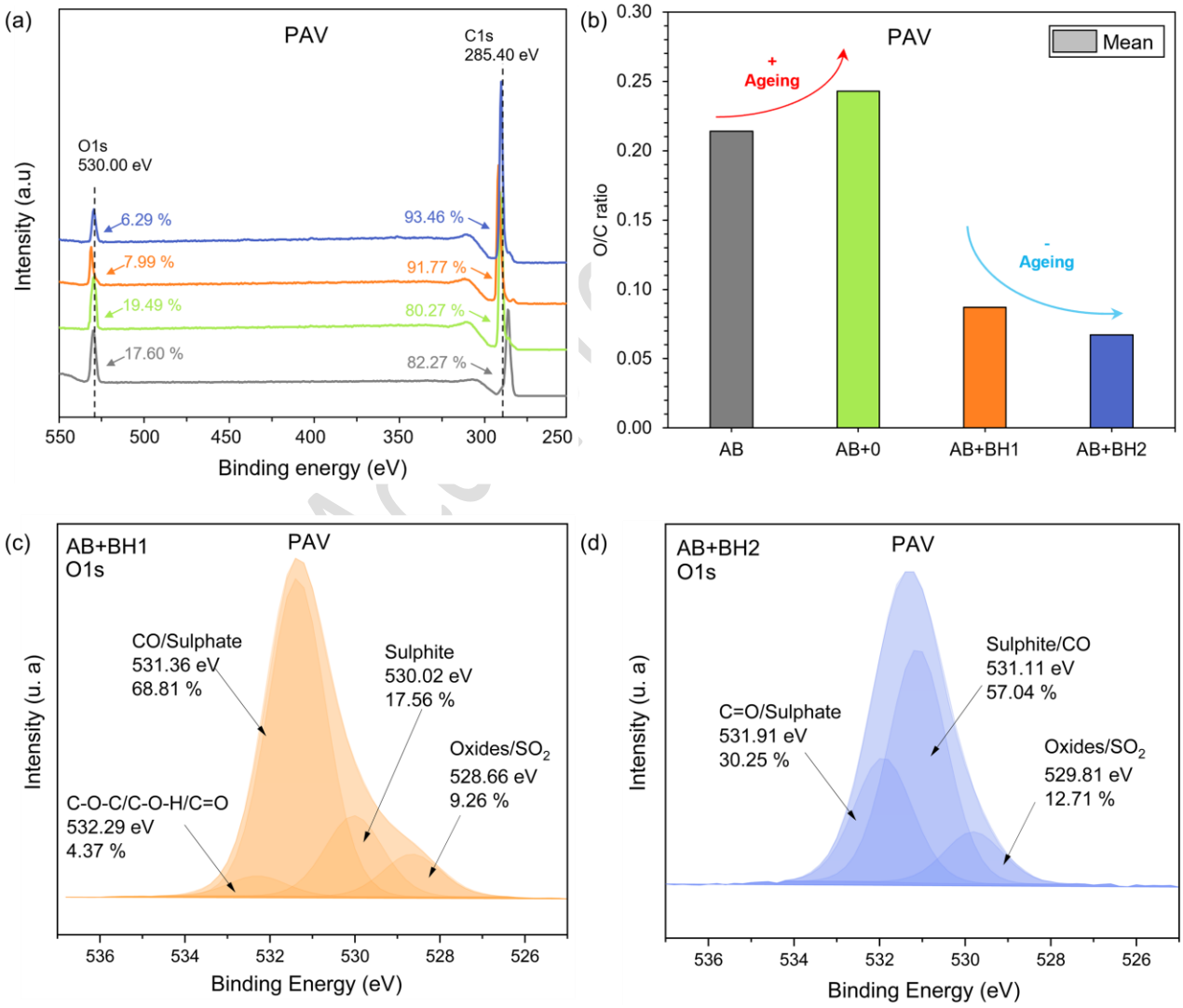

Figure 6. Results of the XPS test on long-term aged (PAV) samples: (a) survey scan between 550 and 250 eV of the samples AB, AB+0, AB+BH1, and AB+BH2; (b) O/C ratio based on the results from Figure 6(a) for the samples AB, AB+0, AB+BH1, and AB+BH2; (c) identification of components in the O1s peak of the AB+BH1 sample; and (d) identification of components in the O1s peak of the AB+BH2 sample.

Regarding the oxygenated chemical components, it should be noted that O1s contributions from C–O, C=O, and S–O bonds partially overlap. Therefore, peak deconvolution reflects relative oxidation environments rather than chemical speciation. Within this framework, the high-resolution O1s spectrum of PAV-aged AB+BH1 (Figure 6(c)) is dominated by CO– and highly oxidised sulphur–oxygen environments (sulphate-like) (68.81 %), followed by sulphite (17.56 %) and minor contributions from C–O–C, C–O–H, and C=O groups. These signals reflect the combined contribution of ageing-related oxidation products, and oxygen-containing functional groups present in BH1 [53], and therefore should not be interpreted as a direct evidence of a higher oxidation state of the asphalt binder itself. In contrast, the O1s spectrum of PAV-aged AB+BH2 (Figure 6(d)) shows a predominance of CO– and moderately oxidised sulphur–oxygen environments (sulphite-like) (57.04 %), followed by C=O/sulphate (30.25 %) and oxides/SO_2 (12.71 %). The lower proportion of highly oxidised sulphate species suggests a comparatively more moderate surface oxidation state relative to AB and AB+0. This behaviour is consistent with the lower oxygen content and higher pyrolysis temperature of BH2, which limit the presence of polar oxygenated functional groups and favour adsorption-driven mitigation of oxidation rather than chemical radical scavenging.

3.2. Effect of biochar on the physical properties of asphalt binder

Recent studies indicate that the most significant effect of applying biochar in asphalt binder modification is observed at high service temperatures [16], [39], [80-83]. For this reason, an analysis of rotational viscosity, including an ageing index (Iag) and mixing and compaction temperatures was conducted and presented in Figure 7. The analysis of unaged asphalt binders (Figure 7(a)) shows that the addition of BH1 and BH2 increased the average rotational viscosity by approximately 31 % compared to AB and AB+0 across all tested temperatures (p-value: < 0.001). No statistically significant differences were detected between AB and AB+0 (p-value: 0.552), nor between AB+BH1 and AB+BH2 (p-value: 0.535). This increase in viscosity is attributed to physical interactions between the asphalt binder and the biochar particles, including adhesive effects associated with their porous and rough morphology [16], [53]. Additionally, interactions involving carbon, oxygen, and hydrogen-containing functional groups may contribute to the observed viscosity increase [53].

After RTFO ageing (Figure 7(b)), the rotational viscosity values of all samples tended to converge. Nevertheless, statistically significant differences were detected (p-value: 0.045). Primarily due to AB+BH2, which exhibited an average viscosity approximately 8 % higher than AB (p-value: 0.005). The remaining pairwise comparisons were not statistically significant (p-value > 0.05). This behaviour is consistent with a reduced susceptibility to short-term ageing-related hardening in the presence of biochar. The higher viscosity observed for the BH-modified binders at this stage may be beneficial for rutting resistance at elevated service temperatures [39], [63], [81], although it may also imply increased stiffness, which should be considered in relation to low-temperature performance.

Following PAV ageing (Figure 7(c)), statistically significant reductions in rotational viscosity were observed for AB+BH1 and AB+BH2 compared with AB and AB+0 (p-value: < 0.001). In particular, BH1 reduced the rotational viscosity by approximately 16% compared with AB and by 25 % compared with AB+0 (p-value: 0.001 vs AB and < 0.001 vs AB+0). In contrast, BH2 exhibited a more moderate reduction of approximately 9 % and 19 %, respectively. The more favourable reduction in viscosity observed in BH1, despite its lower specific surface area compared to BH2, suggests that long-term ageing mitigation is governed not only by physical adsorption phenomena but also by chemical antioxidant mechanisms. In this context, the residual phenolic compounds present in BH1 may contribute to radical scavenging and suppression of oxidation-driven hardening during extended ageing. Conversely, the highly porous morphology of BH2 may favour early-stage adsorption of light fractions, leading to higher stiffness at earlier ageing stages, while offering comparatively less mitigation of long-term hardening. The lower viscosity of BH-modified binders after PAV ageing indicates reduced long-term stiffening and may enhance resistance to cracking in aged pavements, which represents the dominant distress mechanism in later service life stages [63], [84], [85].

When analysing the Iag, Figure 7(d) shows that AB+BH1 and AB+BH2 exhibited the lowest values compared with AB and AB+0, both after RTFO and PAV ageing. Furthermore, no statistically significant differences were detected between AB+BH1 and AB+BH2 (p-value: 0.806 for RTFO and 0.101 for PAV). These results suggest

that the addition of BH1 and BH2 can potentially enhance the ageing resistance of an oxidised asphalt binder [16]. An example of this, the AB+0 sample exhibited the highest Iag values in both RTFO and PAV, indicating that it was the most aged sample. In this case, the reduction in Iag observed in the AB+BH samples is attributed to their antioxidant and morphological properties, limiting the formation of rigid, highly oxygenated structures in the aged asphalt binder. This was corroborated by the carbonyl, sulfoxide and combined index results presented in Figure 5 and the O1s peak analysis shown in Figure 6.

On the other hand, given that BH increases the rotational viscosity of the unaged asphalt binder, the mixing and compaction temperatures were evaluated at 0.17 and 0.28 Pa·s, respectively, according to [43], [63]. In this regard, Figure 7(e) shows that the addition of 5 wt% BH, either BH1 or BH2, raises the mixing and compaction temperatures by approximately 5 °C compared with AB and AB+0. Nevertheless, according to the literature, this increase is lower than that reported in other studies. For instance, Çeloğlu et al. [81], used biochar from walnut shells and apricot seed shells to modify asphalt binder, resulting in mixing and compaction temperatures at least 15 °C higher due to the elevated viscosities achieved after modification.

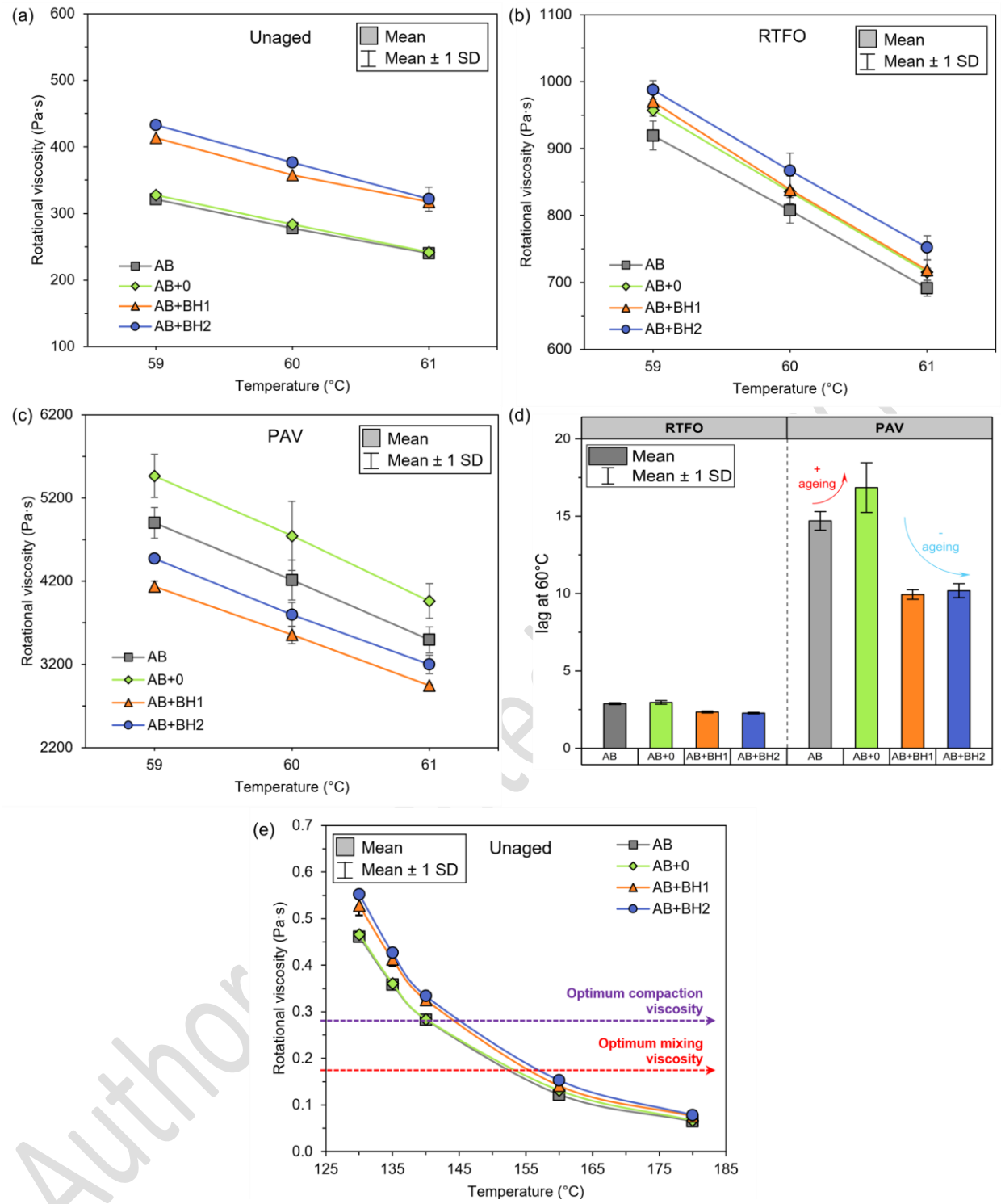

Figure 7. Analysis of the average rotational viscosity results for the samples AB, AB+0, AB+BH1, and AB+BH2: (a) unaged, (b) short-term aged (RTFO), and (c) long-term aged (PAV); (d) Iag obtained at 60 °C based on the rotational viscosity results at 60 °C; and (e) mixing and compaction temperatures according to the optimal rotational viscosity values of 0.17 and 0.28 Pa·s, respectively.

Figure 8 illustrates the high and intermediate temperature behaviour of the asphalt binder through the evaluation of the softening point and penetration at 25 °C, together with the assessment of indices derived from these results. When analysing the change from the semi-solid to the liquid state of the asphalt binders evaluated, Figure 8(a) shows that AB, AB+0, AB+BH1, and AB+BH2 increased their softening point as ageing progressed, reaching the highest softening temperatures after PAV ageing (p-values: < 0.050 for all samples). On average,

AB and AB+0 exhibited the highest softening temperatures, with an increase of approximately 33 % from the unaged state to PAV ageing. In contrast, AB+BH1 and AB+BH2 showed smaller differences, with increases of only about 24 % and 20 %, respectively. In the ageing-state analysis, only the PAV-aged asphalt binders showed statistically significant differences in softening point, with AB+BH1 and AB+BH2 exhibiting the lowest values (*p*-value: 0.004). AB and AB+0 showed similar behaviour (*p*-value: 0.231), indicating that the modification procedure did not affect the softening point of the asphalt binder. Likewise, no statistically significant differences were found between AB+BH1 and AB+BH2 (*p*-value: 0.653), suggesting that pyrolysis temperature did not influence this property. According to the literature, the incorporation of biochar generally increases the softening point of asphalt binder due to its solid particles and interaction with the binder [81], [82]. Furthermore, this increase is usually enhanced by ageing [40]. In this case, the reduction in the softening point observed in PAV-aged asphalt binder is attributed to the presence of BH, which mitigates the long-term ageing effect through two mechanisms: antioxidant properties in BH1 and microscopic morphology in BH2. It should be noted that, although a lower softening point is commonly associated with reduced high-temperature stiffness, this effect is observed here exclusively after PAV ageing. Therefore, the reduced softening point in BH-modified binders reflects a mitigation of ageing-induced over-stiffening rather than an excessively soft material. This interpretation is consistent with the rheological results, which show that BH-modified binders maintain adequate high-temperature performance in unaged and RTFO-aged states, while exhibiting improved performance in the long term.

A preliminary analysis of Figure 8(b) shows that the penetration of AB, AB+0, AB+BH1, and AB+BH2 decreased significantly with the ageing processes, reaching the lowest penetration after PAV ageing (*p*-value: 0.027). This is attributed to the sustained increase of the asphaltene–solid fraction with successive ageing of the asphalt binder, reducing its penetration while increasing its hardness [63]. For the ageing–state analysis, the penetration of AB+BH1 and AB+BH2 decreased significantly in both the unaged state and after RTFO ageing compared with AB and AB+0 (*p*-value: 0.037 for unaged and 0.038 for RTFO, respectively). On average, unaged AB+BH1 and AB+BH2 showed ~ 23 % lower penetration than AB and ~ 20 % lower than AB+0. After RTFO ageing, this decrease was ~ 9 % lower than AB and ~ 7 % lower than AB+0. According to the literature [43], [81], [82], this behaviour is due to the solid BH particles distributed within the asphalt binder matrix, providing greater resistance that limits the penetration depth. In the study led by Gong et al. [40], the addition of 5 wt% DS-510F biochar also reduced asphalt binder penetration. However, the reduction was 17 % compared with the unaged control and 4 % after RTFO ageing. This suggests that BH may produce a harder asphalt binder than DS-510F biochar when used in the same dosage. Regarding PAV ageing, AB, AB+0, AB+BH1, and AB+BH2 maintained the same penetration level (*p*-value: 0.546). This behaviour is attributed to the antioxidant properties of BH1 and BH2, influenced by the pyrolysis temperature, which mitigated the asphalt binder hardening caused by long-term ageing and the presence of BH particles [81]. Complementarily, Figure 8(c) shows that the retained penetration index after RTFO ageing was higher in AB+BH1 and AB+BH2 than in AB and AB+0. This suggests that BH increases asphalt binder hardness, which, in a newly constructed pavement, could contribute to greater structural capacity [43], [54]. Regarding the retained penetration index after PAV ageing, the results were statistically similar among AB, AB+0, AB+BH1, and AB+BH2, consistent with the trends observed in Figure 8(b). This indicates that BH tends to preserve the behaviour of the control asphalt binders despite ageing and the presence of its solid particles, preventing excessive material stiffening.

Figure 8(d) shows the PI results, used as an indicator of the thermal susceptibility of the control binders and the biochar-modified binders in the unaged, RTFO-aged, and PAV-aged states. In unaged binders, the PI reflects their thermal susceptibility, where lower values indicate greater sensitivity to temperature, while higher or more stable values represent lower susceptibility [63], [81]. In this condition, all analysed binders exhibited negative PI values, falling within the typical range of binders used in pavement construction. After ageing, the PI tends to increase as a result of binder hardening. In particular, long-term ageing leads to higher PI values, reflecting a stiffer binder structure with lower apparent thermal susceptibility, but could lead to increased brittleness. In this context, the smaller increase in PI observed in the biochar-modified binders from the RTFO to the PAV condition could indicate greater resistance to ageing, as the presence of biochar mitigates excessive binder hardening. This behaviour suggests that biochar contributes to stabilising the thermal susceptibility of asphalt, limiting oxidation-induced structural changes and promoting a more balanced binder structure, which may translate into reduced brittleness and enhanced durability. For this indicator, both biochars exhibited a similar increase in PI from the RTFO to the PAV condition, indicating that both the biochar with high antioxidant

capacity and the biochar characterised by a high specific surface area contribute comparably to mitigating binder ageing effects.

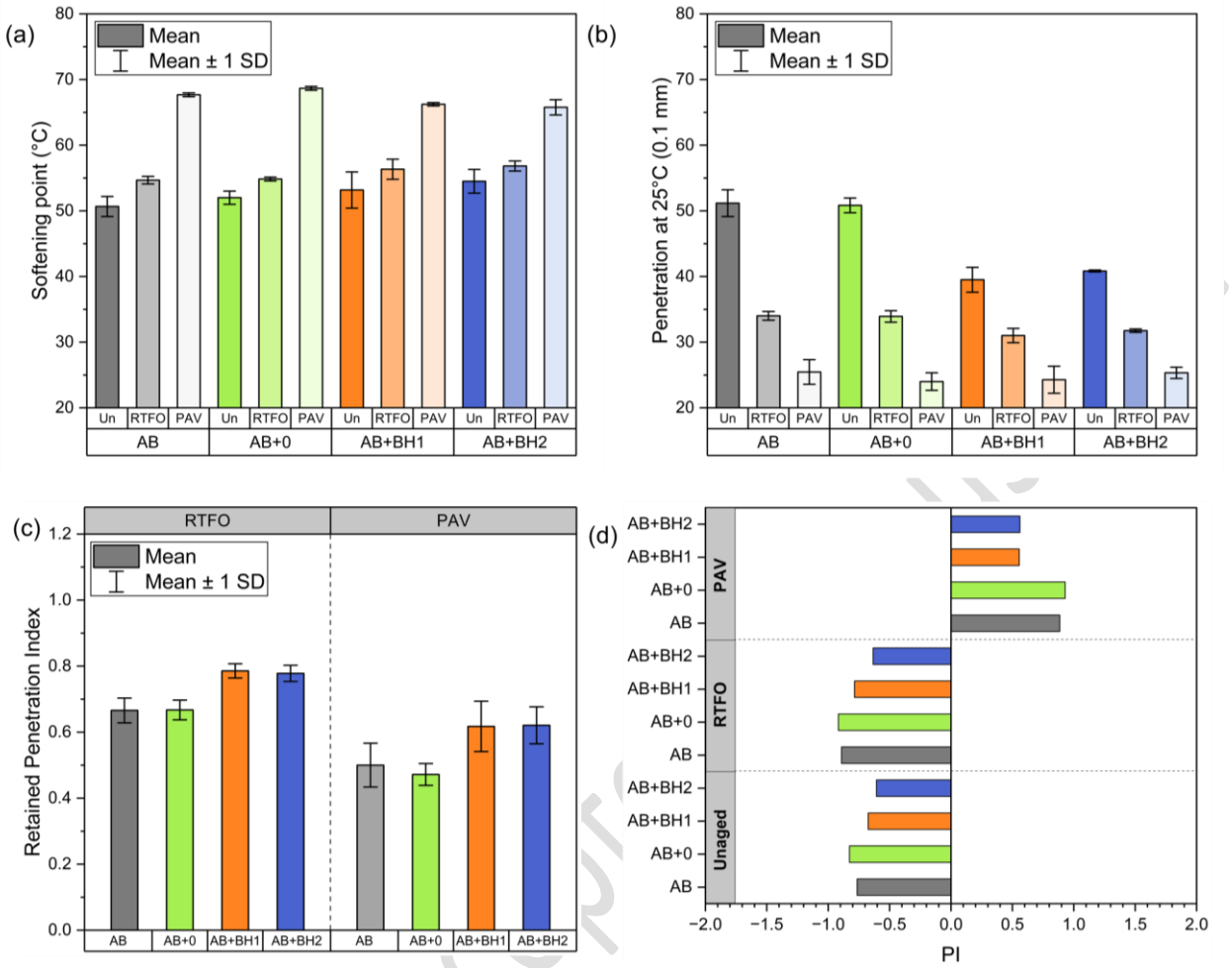

Figure 8. Evaluation of the physical properties of AB, AB+0, AB+BH1, and AB+BH2 at high and intermediate temperatures: (a) softening point in the unaged (Un), short-term aged (RTFO), and long-term aged (PAV) states; (b) penetration at 25 °C in the unaged (Un), short-term aged (RTFO), and long-term aged (PAV) states; (c) retained penetration index derived from the penetration results at 25 °C; and (d) penetration index (PI).

Finally, the Fraass breaking point provides complementary insight into the potential impact of biochar modification on the low-temperature physical properties of the asphalt binders. Figure 9 shows that the Fraass breaking point increased with ageing, causing the PAV-aged samples to fracture at higher temperatures than the unaged and RTFO-aged samples. This behaviour was observed in both the control samples (AB and AB+0), and the biochar-modified asphalt binders. Since AB and AB+0 do not contain an antioxidant modifier, their fractures are attributed to a loss of flexibility caused by the formation of rigid, highly oxygenated structures as a result of ageing [63]. On the other hand, in AB+BH1 and AB+BH2, this behaviour is accentuated by the effect of the solid BH particles. Regarding the ageing state analysis, AB+0, AB+BH1, and AB+BH2 showed slightly higher Fraass breaking points than AB in their unaged, RTFO-aged, and PAV-aged states. Although the differences were statistically significant (p-values of 0.021, 0.016, and 0.014, respectively). This suggests that both the modification process and the presence of BH influenced the temperature at which the asphalt binder becomes brittle. For BH1 and BH2, this effect is attributed to their solid particles with high specific surface areas (BH1: 4.98 m²/g and BH2: 290.72 m²/g [53]) which, in addition to acting as a physical reinforcement within the asphalt binder, may contribute to a loss of flexibility at low temperatures. The increase in the Fraass breaking point was more pronounced for AB+BH2 than for AB+BH1. This behaviour can be mainly attributed to the more developed porous structure and significantly higher specific surface area of BH2, resulting from its

higher pyrolysis temperature (550 °C). Such morphology may favour the physical adsorption of light fractions and maltenes from the asphalt binder, reducing molecular mobility at low temperatures and thereby increasing binder brittleness. Moreover, as these particles are dispersed within the asphalt binder matrix, they may generate stress concentration points that lead to an increase in the Fraass breaking point [53], [83]. These results suggest a moderate reduction in low-temperature flexibility.

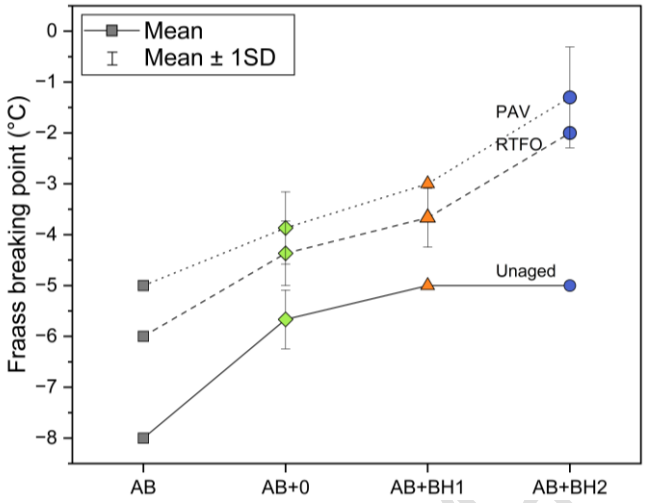

Figure 9. Evaluation of the Fraass breaking point of AB, AB+0, AB+BH1, and AB+BH2 in the unaged, short-term aged (RTFO), and long-term aged (PAV) states, respectively.

3.3. Effect of biochar on the rheological properties of asphalt binder

Figure 10 presents the rheological properties of the asphalt binder evaluated at high service temperatures using the rutting parameter G*/sin(δ) and the RAI. When analysing the unaged asphalt binder, Figure 10(a) shows that AB+BH1 and AB+BH2 exhibited a significantly higher rutting parameter G*/sin(δ) than AB and AB+0 (p-value: < 0.001). At 58 °C, the largest differences were observed: AB+BH1 exceeded the rutting parameter of AB by approximately 8 % and that of AB+0 by around 5 %. Although these differences are moderate in magnitude, they were consistently observed across replicates and exceeded the experimental variability of the DSR measurements, supporting their statistical significance. Regarding the phase angle (δ), AB+BH1 and AB+BH2 displayed viscoelastic behaviour intermediate between AB and AB+0, with AB+0 showing the lowest δ and, consequently, the most elastic response. In this case, no statistically significant differences were found between the phase angles of AB+BH1 and AB+BH2 (p-value: 0.171). Overall, the increase in the rutting parameter together with the reduction in phase angle in the unaged asphalt binder is attributed to the physical reinforcement provided by BH and to its physicochemical interaction with the asphalt binder [39], [44], [53], in agreement with the rotational viscosity analysis shown in Figure 7(a).

With RTFO ageing, Figure 10(b) shows that AB+BH1 and AB+BH2 again exhibited significantly higher rutting parameters G*/sin(δ) than AB and AB+0 (p-value: < 0.001). Meanwhile, their phase angles (δ) remained the same as those of AB (p-value: 0.304). This indicates that the addition of BH increased the complex modulus, and thus the overall stiffness of the asphalt binder, without compromising its deformation capacity. This enhancement in stiffness is attributed to the presence of solid BH particles, which act as physical reinforcement, an effect that outweighs the influence of oxidation, which tends to embrittle asphalt and consequently reduce the phase angle.

It is noted that all binders satisfied the Superpave minimum G/sin(δ) requirement in the unaged state and in the RTFO-aged state. Besides, the differences observed among binders reflect relative changes in stiffness and ageing sensitivity rather than a modification of the High PG grade with respect to the control binder.

On the other hand, Figure 10(c) shows that following PAV ageing, AB+BH1 and AB+BH2 exhibited a significant decrease in the rutting parameter G*/sin(δ) compared to AB and AB+0, along with an increase in

their phase angle (δ) (p-value: 0.001 and < 0.001, respectively). This indicates a beneficial effect of the antioxidant properties of BH1 and BH2 on the rheological behaviour of long-term aged asphalt binder, as pavements with extended service life aim to reduce binder stiffness and enhance viscous behaviour to mitigate cracking caused by ageing [63].

When analysing the RAI shown in Figure 10(d), the results indicate that after ageing by RTFO, AB+BH1 and AB+BH2 exhibited slightly higher values than AB and AB+0. However, after PAV ageing, both AB+BH1 and AB+BH2 showed a significantly lower RAI, approximately 14% lower than AB and between 18 % and 19 % lower than AB+0 (p-value: < 0.001). These findings indicate that the addition of BH1 and BH2 produces an asphalt binder with a reduced susceptibility to long-term ageing, as reflected by lower RAI values after PAV ageing, compared to AB and AB+0 [44], [66], [86]. Although the magnitude of the RAI reduction may be moderate, it is consistent for both biochar types and aligned with other ageing-related indicators discussed in this study.

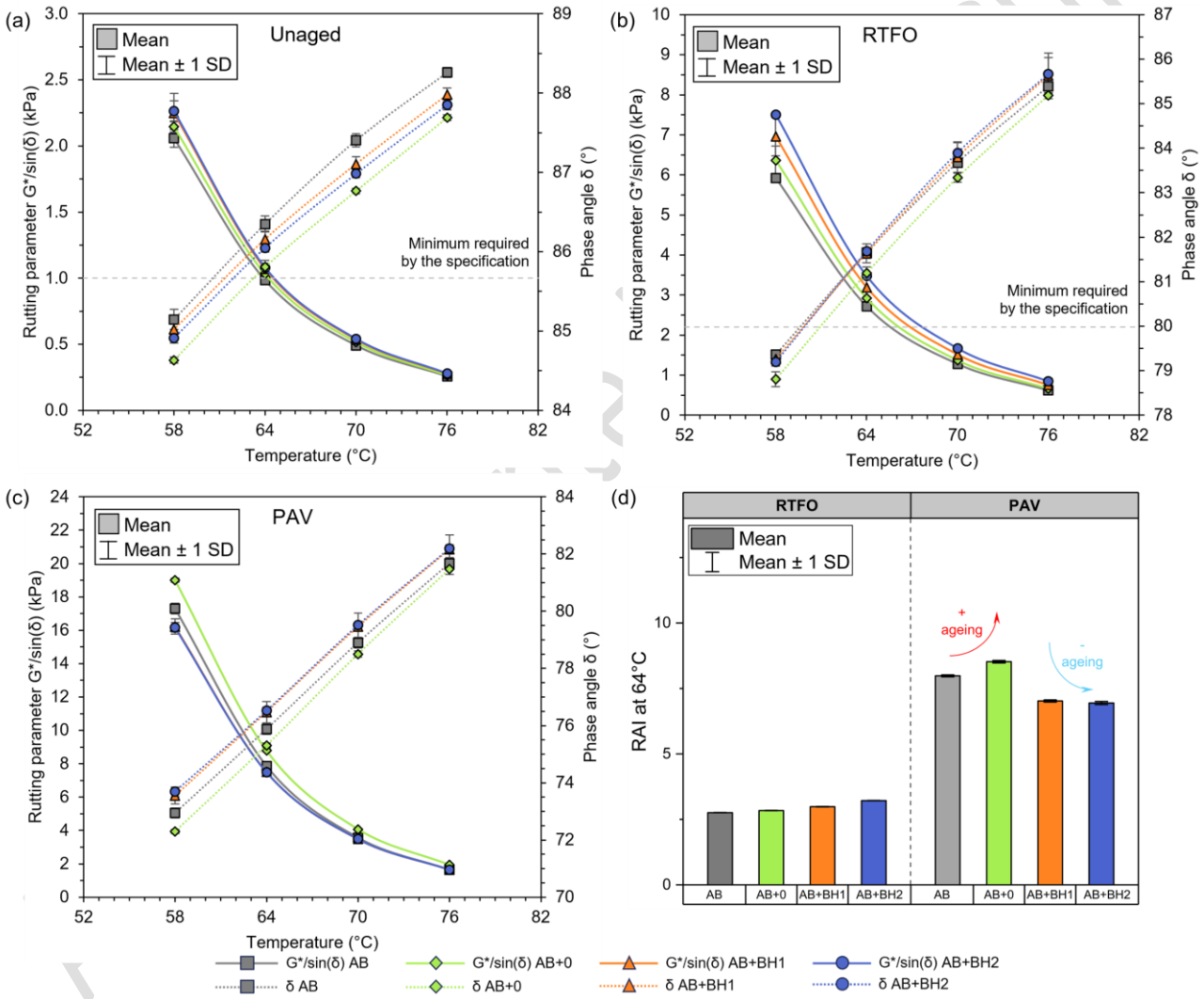

Figure 10. Evaluation of the rutting parameter G*/sin(δ) for AB, AB+0, AB+BH1, and AB+BH2: (a) unaged, (b) short-term aged (RTFO), and (c) long-term aged (PAV); and (d) RAI based on the rutting parameter G*/sin(δ) obtained at 64 °C.

The effect of BH on the viscoelastic properties related to permanent deformation and recovery of the asphalt binder at high temperature was evaluated using the MSCR test. The results are presented in Figure 11. Figure 11(a) and (b) show the strain evolution during each creep–recovery cycle at stress levels of 0.1 kPa (between 100 and 200 s) and 3.2 kPa (between 200 and 300 s), respectively. At the lower stress level of 0.1 kPa, both

AB+BH1 and AB+BH2 exhibited significantly lower strain than the control binders, AB and AB+0 (p-value: 0.010). This behaviour indicates that both biochars induce a comparable stiffening effect under low stress conditions. Consistently, the *Jnr* values at 0.1 kPa (Figure 11(c)) were similar for AB+BH1 and AB+BH2 and approximately 12 – 15 % lower than those of AB and AB+0 (p-value: 0.007), while both biochar-modified binders also showed significantly higher recovery values R (p-value: 0.001). Under these conditions, the MSCR parameters primarily reflect the increased resistance to deformation associated with the presence of solid biochar particles.

When the applied stress increased to 3.2 kPa, entering a non-linear viscoelastic regime, clear differences emerged between the two biochars. As shown in Figure 11(b) and (d), AB+BH1 exhibited significantly lower strain and *Jnr* values than AB and AB+0, with a reduction in *Jnr* of approximately 11 – 12 % (p-value: 0.045). In contrast, AB+BH2 showed a response comparable to the control binders, with no statistically significant reduction in *Jnr*. This behaviour highlights the higher sensitivity of the MSCR test to rheological stability and damage accumulation under repeated loading. The superior performance of BH1 at higher stress levels may be attributed to its higher antioxidant capacity, which preserves the colloidal structure of the asphalt binder and reduces the evolution of viscoplastic damage under repeated creep-recovery cycles.

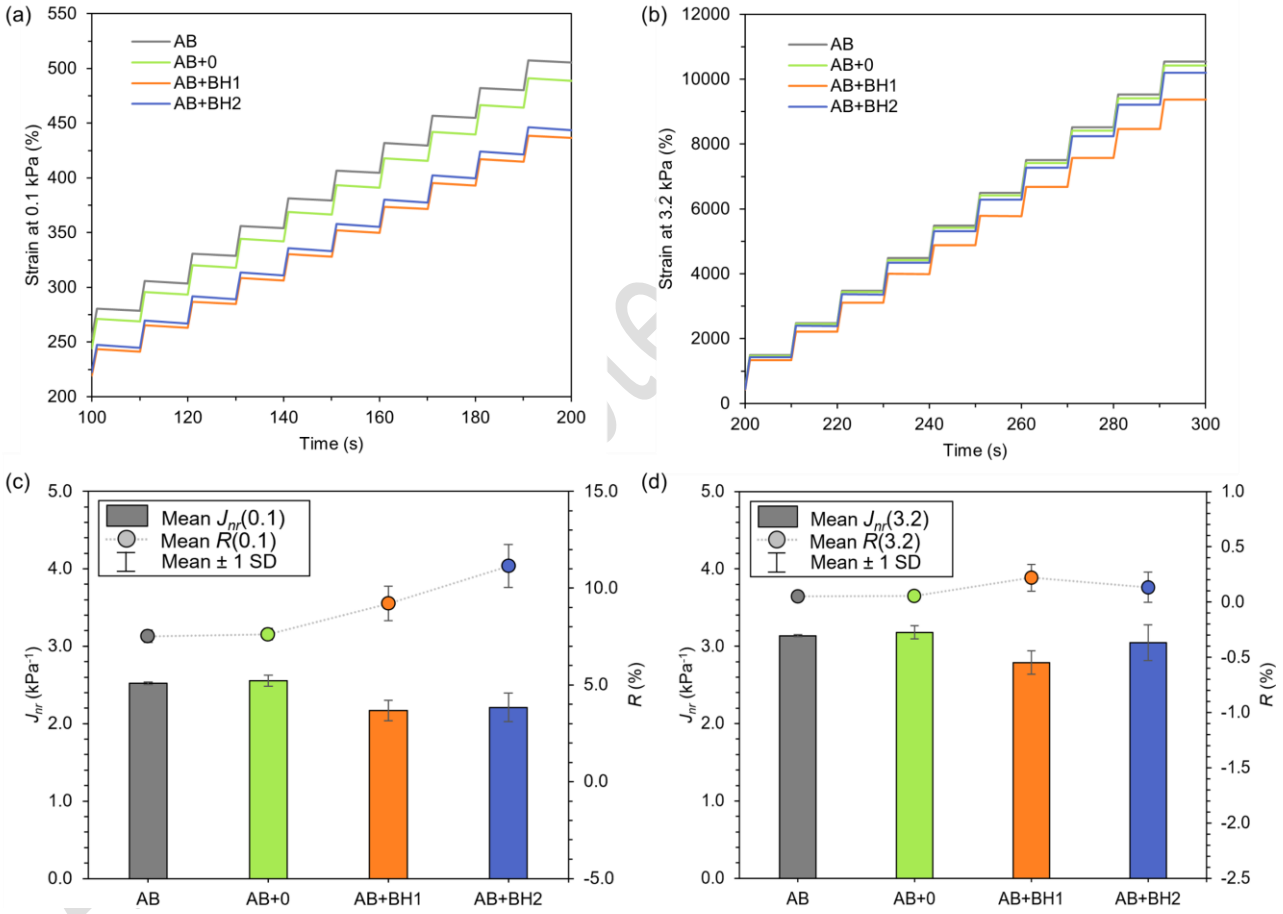

Figure 11. Results of the MSCR test for samples AB, AB+0, AB+BH1, and AB+BH2: (a) strain between 100 and 200 seconds at a stress level of 0.1 kPa; (b) strain between 200 and 300 seconds at a stress level of 3.2 kPa; (c) *Jnr* and R at a stress level of 0.1 kPa; and (d) *Jnr* and R at a stress level of 3.2 kPa.

Regarding PG specification, all binders satisfied the requirements of AASHTO M332 [89], exhibiting *Jnr,diff* values below 75 % at 64 °C. Based on the *Jnr* values obtained at 3.2 kPa, both the control and BH-modified binders were classified within the standard traffic level "S" (Table 5). Nevertheless, the lower *Jnr* observed for AB+BH1 at high stress levels suggests enhanced resistance to permanent deformation under demanding traffic and temperature conditions.

Table 5. Selection of the traffic level based on the results of the MSCR test.

	AB	**AB+0**	**AB+BH1**	**AB+BH2**
$J_{nr,diff}$ (%)	24.39 ± 0.69	24.40 ± 0.20	28.69 ± 1.29	37.87 ± 2.20
Traffic level	S	S	S	S

Note: "S": standard traffic level.

Regarding the evaluation of rheological properties at intermediate temperatures, Figure 12 presents the results of the fatigue parameter G*·sin(δ) for asphalt binders in unaged, RTFO-aged, and PAV-aged conditions. Figure 12(a) and (b) show that for the unaged state and after RTFO ageing, both AB+BH1 and AB+BH2 exhibited slightly higher fatigue parameters compared to AB and AB+0 across the temperature range evaluated. These differences were statistically significant, with *p*-values of 0.026 for the unaged state and 0.011 for the RTFO-aged condition. This effect was most pronounced at 16 °C, where AB+BH1 demonstrated a fatigue parameter approximately 8 % higher than AB and 9 % higher than AB+0 in the unaged state. Following RTFO ageing, these differences were about 6 % and 8 %, respectively, with similar results observed for AB+BH2. Typically, the fatigue parameter is assessed in long-term aged asphalt binders; however, in this case, its evaluation in both unaged and RTFO-aged states facilitates the characterisation of the initial fatigue susceptibility of the asphalt modified with BH.

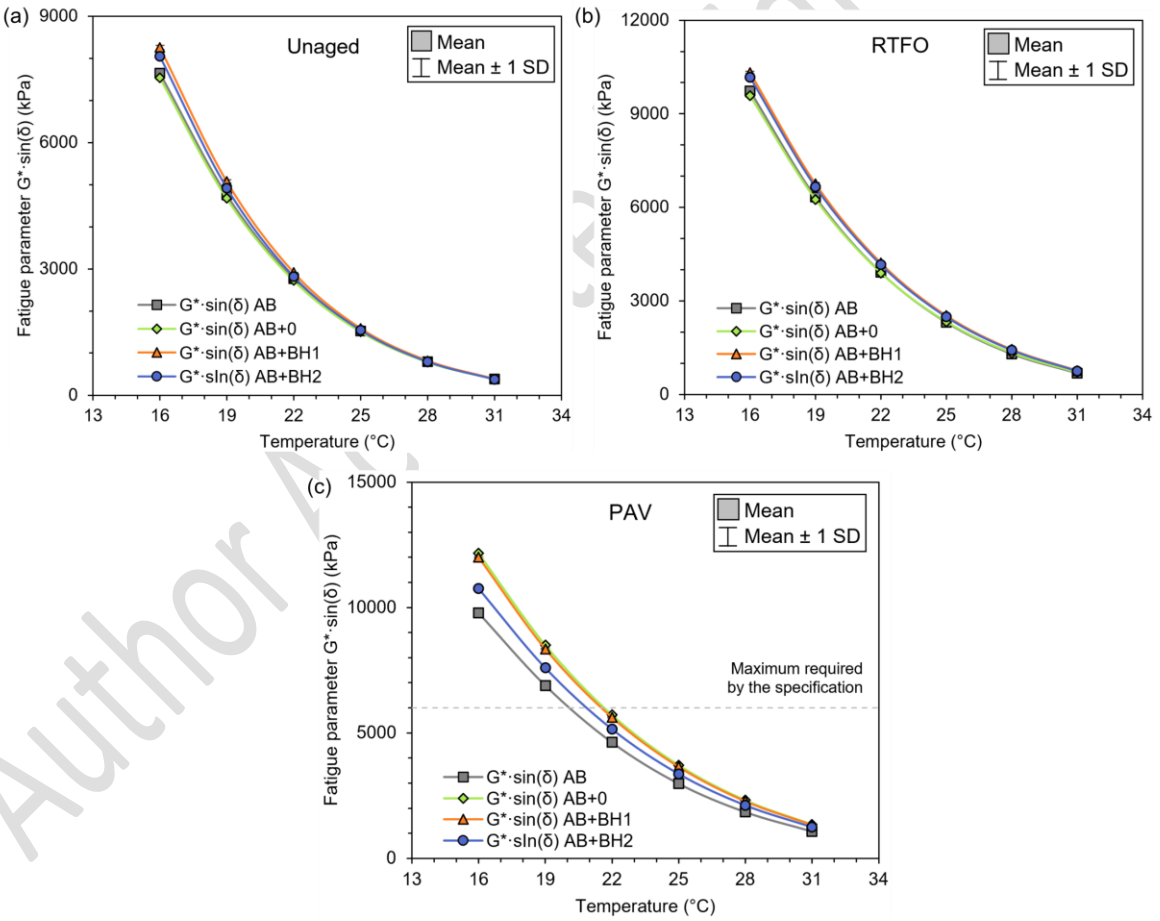

Figure 12. Evaluation of the fatigue parameter G*·sin(δ) of AB, AB+0, AB+BH1, and AB+BH2 in the states of: (a) unaged, (b) short-term aged (RTFO), and (c) long-term aged (PAV).

Regarding long-term ageing by PAV, Figure 12(c) shows that AB+BH1 and AB+BH2 exhibited fatigue parameter values situated between those of AB and AB+0. In this regard, AB+BH1 demonstrated behaviour similar to AB+0, whereas AB+BH2 presented a fatigue parameter approximately 12 % higher than AB and

10 % lower than AB+0, considering the average across all evaluated temperatures. These differences were statistically significant (p-value: 0.026 in relation to both AB and AB+0). The observed increase in the fatigue parameter may be associated with a higher complex modulus, attributed both to the modification procedure and the incorporation of solid biochar particles. Several studies report that the use of biochars enhances fatigue resistance, particularly when particles smaller than 20 µm are employed in combination with optimal additive contents [83]. Additionally, Figure 12(c) also shows that AB, AB+0, AB+BH1, and AB+BH2 complied with the PG specification by achieving a fatigue parameter G*·sin(δ) below 6000 kPa at the intermediate temperature of 25 °C.

To complement the analysis at intermediate temperatures, the fatigue-related rheological behaviour of the asphalt binder was assessed using the Tcross, defined as the temperature at which the storage modulus (G′) equals the loss modulus (G″), Figure 13(a). This parameter represents a rheological transition associated with the balance between elastic and viscous responses of the binder. Below Tcross, the asphalt binder exhibits a more elastic-dominated response, which has been associated with increased susceptibility to fatigue cracking [69], [70]. As shown in Figure 13(b), although the fatigue parameter G*·sin(δ) increased relative to AB (Figure 12), the incorporation of BH1 and BH2 did not lead to statistically significant differences in Tcross for the PAV-aged binders (p-value: 0.435). The transition temperature remained close to 25 °C for all binders, including AB and AB+0. This indicates that the addition of biochar did not modify the viscoelastic balance of the asphalt binder in the long term, but rather influenced stiffness-related parameters without shifting the elastic–viscous transition.

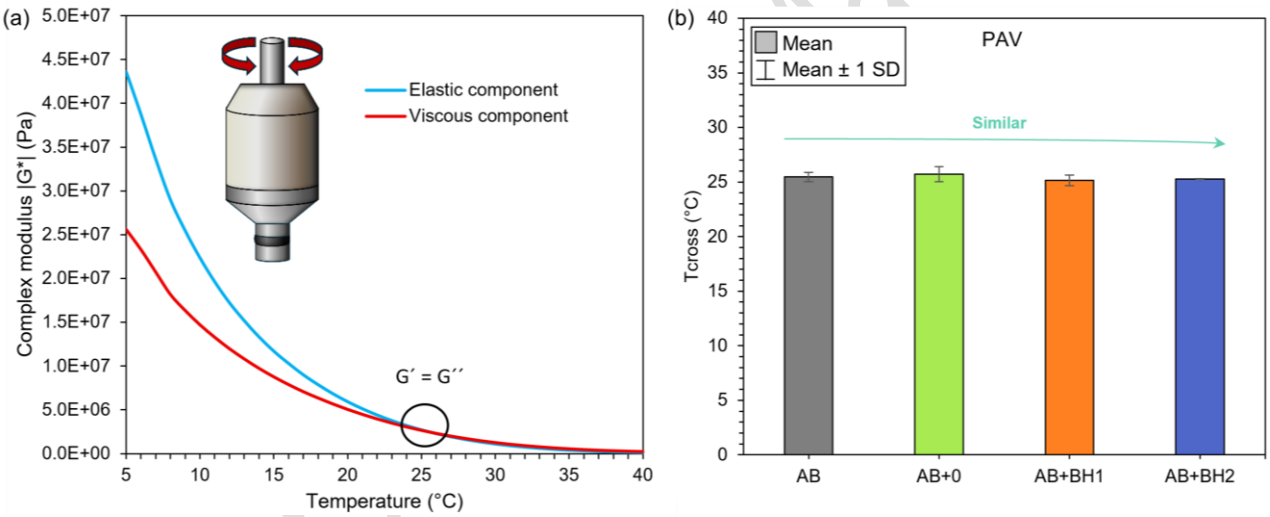

Figure 13. Evaluation of the Tcross of AB, AB+0, AB+BH1, and AB+BH2: (a) intersection between the elastic and viscous components of the asphalt binder, and (b) Tcross of the asphalt binders aged long-term (PAV).

Regarding the evaluation of rheological properties at low service temperatures, Figure 14 presents the results of the complex modulus (|G*|) for AB, AB+0, AB+BH1, and AB+BH2 in their unaged state (Figure 14(a)), short-term aged by RTFO (Figure 14(b)), and long-term aged by PAV (Figure 14(c)), measured at -10 °C. Additionally, the increase in |G*| from the unaged state to the PAV-aged state is also shown in Figure 14(d).

A general analysis shows that ageing through the RTFO and PAV processes caused an increase in |G*|, indicating a rise in the overall stiffness of the asphalt binders. Figure 14(a) reveals that the unaged AB exhibited the lowest |G*|, followed by AB+0, AB+BH1, and AB+BH2. Through the modification process, the |G*| for the unaged AB+0 increased by approximately 11 % compared to AB, reaching statistically significant differences (p-value: < 0.001). This behaviour persisted with ageing by RTFO and PAV. It is also observed that with the application of BH1 and BH2, the |G*| values increased by around 20 % and 22 %, respectively, compared to AB. This result was attributed to a combination of the stiffening effect caused by the modification process and the solid particles of BH.

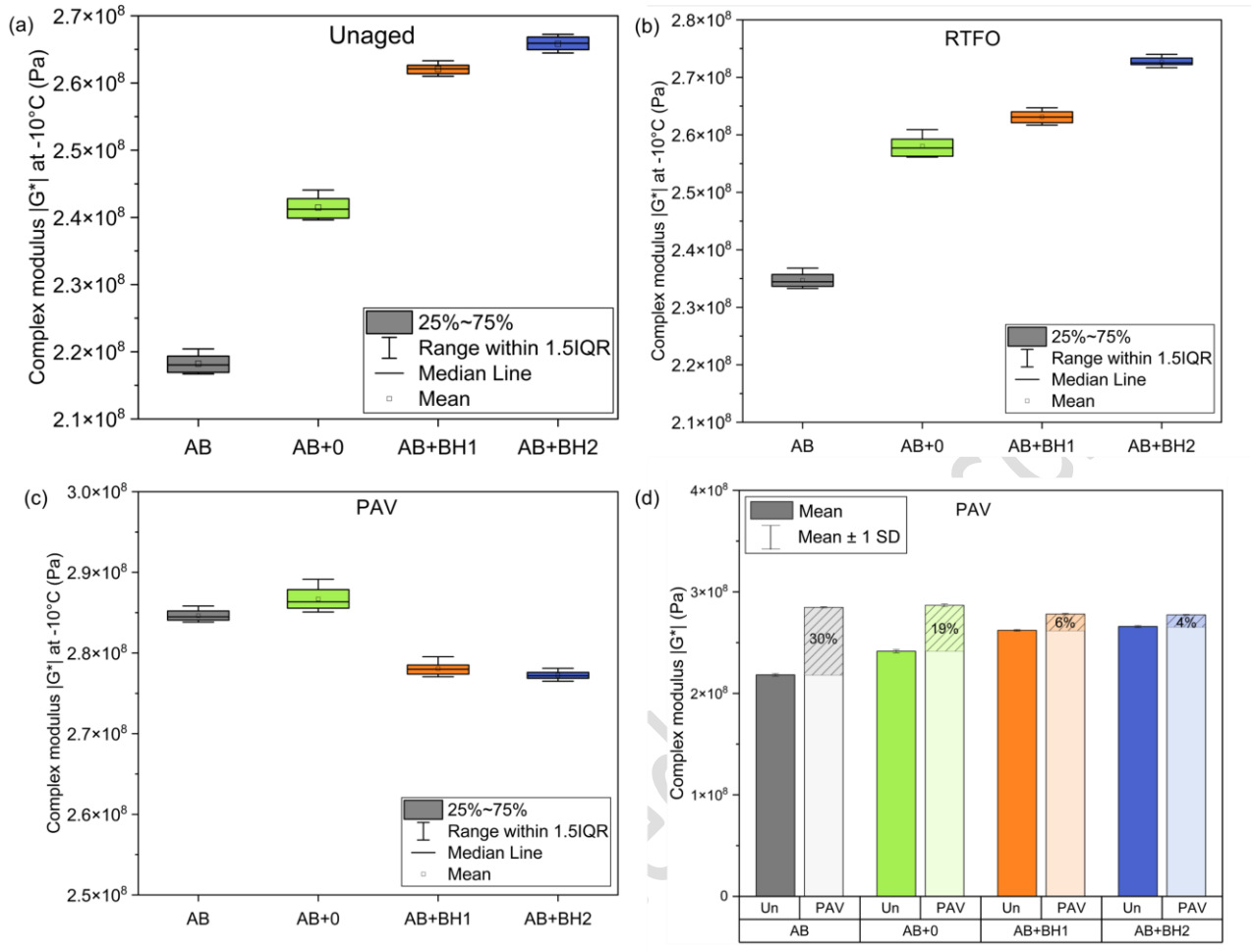

Figure 14. Evaluation of the complex modulus (|G*|) at -10°C for AB, AB+0, AB+BH1, and AB+BH2 in the following states: (a) unaged, (b) short-term aged (RTFO), and (c) long-term aged (PAV); (d) increase in complex modulus from the unaged state (Un) to the PAV-aged state.

With RTFO ageing, the |G*| of AB remained the lowest compared to the other samples in Figure 14(b). However, under this ageing condition, the |G*| of AB+BH1 was slightly higher than that of AB+0, indicating a reduction in stiffness attributed to the antioxidant effect of BH1. Conversely, AB+BH2 continued to exhibit the highest |G*|, being approximately 16 % higher than AB and 6 % higher than AB+0.

Figure 14(c) presents the most significant results regarding the antioxidant effect of BH on PAV-aged asphalt binders, evidenced by a reduction in the |G*|. Both AB+BH1 and AB+BH2 exhibited a |G*| approximately 3 % lower than that of AB and AB+0, with statistically significant differences (p-value: < 0.001). This indicates that, despite the ageing process and the presence of solid modifier particles, BH1 and BH2 effectively reduce the overall stiffness of the asphalt binder at the critical temperature of -10 °C, which is even lower than the Fraass breaking point of the PAV-aged binders (Figure 9(b)). Based on these findings, it is inferred that fewer oxidation and volatilisation mechanisms of volatile organic compounds occurred in AB+BH1 and AB+BH2 compared to AB and AB+0 due to the addition of BH.

On the other hand, Figure 14(d) shows that the variation in complex modulus from the unaged state to the PAV-aged state was smaller in the asphalt binders containing BH. Specifically, AB+BH1 and AB+BH2 exhibited changes in |G*| of approximately 6 % and 4 %, respectively. In contrast, AB and AB+0 showed variations of around 30 % and 19 %, respectively. Comparing these results with the sulfoxide, carbonyl, and combined indices presented in Figure 5, it can be concluded that the oxidative contribution due to the addition of BH1 and

BH2 is mitigated through the successive RTFO and PAV ageing processes. This reduction is attributed to the antioxidant properties derived from phenolic compounds (Table 3) and the microscopic morphology (Table 1) of BHs, respectively.

4. Conclusions

This study assessed the impact of biochars derived from European hazelnut shells on the antioxidant, physical, and rheological properties of asphalt binder in its unaged state, following short-term ageing (RTFO), and after long-term ageing (PAV). Based on the experimental results, the following conclusions were drawn:

- Slow pyrolysis leads to the partial degradation of phenolic compounds in European hazelnut shells, resulting in a reduction of the antioxidant capacity of the produced biochars. Nevertheless, a fraction of these phenolic compounds is retained in biochar pyrolysed at 300 °C with a residence time of 1 h (BH1). Furthermore, these pyrolysis conditions may promote the formation of new phenolic compounds within the biochar.

- At the chemical level, both BH1 (300 °C) and BH2 (550 °C) exhibited antioxidant effects on the asphalt binder, as evidenced by lower FTIR-ATR indices (carbonyl, sulfoxide, combined, and antioxidant) and a reduction in the O1s peak and O/C ratio measured by XPS. While the decrease in the O/C ratio partly reflects the carbonaceous nature of the biochars, its consistent agreement with FTIR ageing indices supports its interpretation as an indicator of reduced oxidation in the binder. The antioxidant effect of BH1 was attributed to its phenolic compounds, whereas that of BH2 was associated with its highly developed porous morphology, which may facilitate the adsorption of volatile organic compounds during high temperature exposure. As a result, BH2 exhibited a more pronounced antioxidant effect during the early state of ageing. However, both biochars showed comparable long-term ageing mitigation.

- At the physical level, rotational viscosity test showed that except in unaged and RTFO states, BH1 and BH2 reduced viscosity in PAV-aged binders, making them less susceptible to long-term ageing. The antioxidant effect of the biochars is also reflected in the retention of penetration at 25 °C and the reduction in the softening point (compared with the control binders) after PAV ageing. Conversely, the increase in the Fraass breaking point in unaged, RTFO-aged, and PAV-aged asphalt binders was predominantly influenced by the stiffening effect of the solid biochar particles. Taken together, these results highlight an performance trade-off between enhanced ageing resistance and high-temperature behaviour and a moderate reduction in low-temperature flexibility.

- At the rheological level, the incorporation of biochar increased binder stiffness and rutting resistance in the unaged and RTFO-aged states, as reflected by higher $G^*/\sin(\delta)$ values. However, after PAV ageing, biochar-modified binders exhibited lower stiffness and higher phase angles compared to the control binders, indicating mitigation of ageing-induced hardening. This behaviour is consistent with the trends observed in the RAI and MSCR parameters, which suggest that while biochar limits long-term stiffness evolution, it does not significantly enhance elastic recovery due to the solid nature of the particles. Fatigue-related parameters ($G^* \cdot \sin(\delta)$ and Tcross) further indicate that biochar offsets excessive stiffness development after long-term ageing, contributing to the preservation of the viscoelastic response of the binders. At low service temperatures, biochar incorporation reduced the evolution of stiffness between the unaged and PAV-aged states, although a moderate increase in stiffness was observed in the unaged and RTFO-aged conditions.

The findings presented in this study are limited to binder-scale characterisation and should therefore be interpreted within this context. In addition, the reported trends and the comparative performance of BH1 and BH2 are specific to the selected biochar dosage (5 wt%). Performance at the mixture level and field validation are necessary to confirm the applicability of the observed ageing mitigation effects under real pavement conditions. These aspects are identified as key directions for future research. Furthermore, economic, technical, environmental, and social assessments are relevant studies to be conducted in future research to support industrial scalability.

5. Funding

This research was funded by the National Research and Development Agency (ANID) from the Government of Chile, through the Research Project FONDECYT Regular 2023 No. 1230035.

6. Acknowledgements

The first author gratefully acknowledges the financial support provided by the National Research and Development Agency (ANID) of the Government of Chile through his PhD scholarship No. 21230892. The authors also wish to thank José Dario Nahuel, Isabel Riquelme, and Luis Muñoz for their invaluable assistance throughout the experimental programme.

7. Declaration of generative AI and AI-assisted technologies in the writing process

During the preparation of this work, the authors used ChatGPT in order to enhance the readability and grammar of the text. After using this tool, the authors reviewed and edited the content as needed and take full responsibility for the content of the publication.

References

[1] C. Chen, X. Quan, C. Ge, T. Ma, X. Wang, and Y. Zhang, "Laboratory evaluation of canola oil modified hard asphalt binders with different oleic acid contents: Rheological properties and microscopic characteristics," *J Mol Liq*, vol. 413, Nov. 2024, doi: 10.1016/j.molliq.2024.125927.

[2] EAPA, "Learn about asphalt." Accessed: Dec. 04, 2024. [Online]. Available: https://eapa.org/asphalt/

[3] Wangjie. Wu, H. Li, O. Sevastyanova, N. Kringos, and M. C. Cavalli, "Exploring the physicochemical and rheological properties of sustainable asphalt binders modified with lignin and high-viscosity additive," *Constr Build Mater*, vol. 450, Nov. 2024, doi: 10.1016/j.conbuildmat.2024.138621.

[4] C. Peng *et al.*, "Effect of a lignin-based polyurethane on adhesion properties of asphalt binder during UV aging process," *Constr Build Mater*, vol. 247, Jun. 2020, doi: 10.1016/j.conbuildmat.2020.118547.

[5] H. Yu *et al.*, "Impact of ultraviolet radiation on the aging properties of SBS-modified asphalt binders," *Polymers (Basel)*, vol. 11, no. 7, 2019, doi: 10.3390/polym11071111.

[6] R. Luo, H. Liu, and Y. Zhang, "Characterization of linear viscoelastic, nonlinear viscoelastic and damage stages of asphalt mixtures," *Constr Build Mater*, vol. 125, pp. 72–80, Oct. 2016, doi: 10.1016/j.conbuildmat.2016.08.039.

[7] T. Li, K. Jiang, K. Liu, and Q. Li, "Fourier transform infrared spectroscopy characterization of aging properties of graphene oxide modified asphalt binder," *Int J Adhes Adhes*, vol. 139, May 2025, doi: 10.1016/j.ijadhadh.2025.103974.

[8] Y. J. Xie, Q. Fu, K. R. Zheng, Q. Yuan, and H. Song, "Dynamic mechanical properties of cement and asphalt mortar based on SHPB test," *Constr Build Mater*, vol. 70, pp. 217–225, Nov. 2014, doi: 10.1016/j.conbuildmat.2014.07.092.

[9] Q. Zheng, P. He, D. Zhang, Y. Weng, J. Lu, and T. Wang, "A Holistic View of Asphalt Binder Aging under Ultraviolet Conditions: Chemical, Structural, and Rheological Characterization," Oct. 01, 2024, *Multidisciplinary Digital Publishing Institute (MDPI)*. doi: 10.3390/buildings14103276.

[10] Y. L. Yaphary, Z. Leng, H. Wang, S. Ren, and G. Lu, "Characterization of nanoscale cracking at the interface between virgin and aged asphalt binders based on molecular dynamics simulations," *Constr Build Mater*, vol. 335, Jun. 2022, doi: 10.1016/j.conbuildmat.2022.127475.

[11] M. E. Abdullah *et al.*, "Effects of Kaolin Clay on the Mechanical Properties of Asphaltic Concrete AC14," in *IOP Conference Series: Earth and Environmental Science*, Institute of Physics Publishing, Apr. 2018. doi: 10.1088/1755-1315/140/1/012121.

[12] H. Ji, B. Li, T. Yao, Z. Liu, J. Han, and A. Li, "Polyurethane and nano-TiO2 modifiers mitigate aging of asphalt binders by inhibiting aggregation of polar molecules: A molecular dynamics study," *Colloids Surf A Physicochem Eng Asp*, vol. 679, Dec. 2023, doi: 10.1016/j.colsurfa.2023.132654.

[13] C. Zhu, D. Li, H. Zhang, Z. Wang, and J. Li, "Synergistic effect of surface modified nano-zinc oxide and organic vermiculite on long-term ultraviolet and thermal-oxidative aging resistance of different asphalt binders," *Constr Build Mater*, vol. 409, Dec. 2023, doi: 10.1016/j.conbuildmat.2023.133832.

[14] R. Wang, Z. Qi, R. Li, and J. Yue, "Investigation of the effect of aging on the thermodynamic parameters and the intrinsic healing capability of graphene oxide modified asphalt binders," *Constr Build Mater*, vol. 230, Jan. 2020, doi: 10.1016/j.conbuildmat.2019.116984.

[15] P. Pan, S. Wu, Y. Xiao, P. Wang, and X. Liu, "Influence of graphite on the thermal characteristics and anti-ageing properties of asphalt binder," *Constr Build Mater*, vol. 68, pp. 220–226, Oct. 2014, doi: 10.1016/j.conbuildmat.2014.06.069.

[16] R. Zhang, Q. Dai, Z. You, H. Wang, and C. Peng, "Rheological performance of bio-char modified asphalt with different particle sizes," *Applied Sciences (Switzerland)*, vol. 8, no. 9, Sep. 2018, doi: 10.3390/app8091665.

[17] P. Cong, P. Xu, and S. Chen, "Effects of carbon black on the anti aging, rheological and conductive properties of SBS/asphalt/carbon black composites," *Constr Build Mater*, vol. 52, pp. 306–313, Feb. 2014, doi: 10.1016/j.conbuildmat.2013.11.061.

[18] K. Zhong, Z. Li, J. Fan, G. Xu, and X. Huang, "Effect of carbon black on rutting and fatigue performance of asphalt," *Materials*, vol. 14, no. 9, May 2021, doi: 10.3390/ma14092383.

[19] European Commission, "European Green Deal." Accessed: Apr. 19, 2023. [Online]. Available: Pacto Verde Europeo

[20] United Nations, "The Sustainable Development Goals Report 2024," 2024. Accessed: Dec. 31, 2024. [Online]. Available: https://unstats.un.org/sdgs/report/2024/

[21] S. Baradaran, M. R. M. Aliha, A. Maleki, and B. S. Underwood, "Fracture properties of asphalt mixtures containing high content of reclaimed asphalt pavement (RAP) and eco-friendly PET additive at low temperature," *Constr Build Mater*, vol. 449, Oct. 2024, doi: 10.1016/j.conbuildmat.2024.138426.

[22] M. Yu, D. Jin, Y. Liu, Z. You, and Y. Li, "Performance evaluation of surface treatment waste glass as aggregate in asphalt mixture," *Case Studies in Construction Materials*, vol. 21, Dec. 2024, doi: 10.1016/j.cscm.2024.e03767.

[23] G. Valdés-Vidal, A. Calabi-Floody, C. Duarte-Nass, C. Mignolet, and C. Díaz, "Development of a New Additive Based on Textile Fibers of End-of-Life Tires (ELT) for Sustainable Asphalt Mixtures with Improved Mechanical Properties," *Polymers (Basel)*, vol. 14, no. 16, Aug. 2022, doi: 10.3390/polym14163250.

[24] R. Potnuri, D. V. Surya, C. S. Rao, A. Yadav, V. Sridevi, and N. Remya, "A review on analysis of biochar produced from microwave-assisted pyrolysis of agricultural waste biomass," *J Anal Appl Pyrolysis*, vol. 173, Aug. 2023, doi: 10.1016/j.jaap.2023.106094.

[25] A. Martinez-Soto, G. Valdes-Vidal, A. Calabi-Floody, C. Avendaño-Vera, and C. Martínez-Toledo, "Comparison of Environmental Loads of Fibers Used in the Manufacture of Hot Mix Asphalt (HMA) and Stone Mastic Asphalt (SMA) Mixes Using a Life Cycle Assessment (LCA)," *Sustainability*, vol. 14, no. 21, p. 14246, Nov. 2022, doi: 10.3390/su142114246.

[26] S. Baradaran and M. Ameri, "Durable and sustainable warm mix asphalt pavement using value-added recycled PET," *Case Studies in Construction Materials*, vol. 23, Dec. 2025, doi: 10.1016/j.cscm.2025.e05362.

[27] K. Wu *et al.*, "Enhancing levoglucosan production from waste biomass pyrolysis by Fenton pretreatment," *Waste Management*, vol. 108, pp. 70–77, May 2020, doi: 10.1016/j.wasman.2020.04.023.

[28] V. Dhyani and T. Bhaskar, "A comprehensive review on the pyrolysis of lignocellulosic biomass," *Renew Energy*, vol. 129, pp. 695–716, Dec. 2018, doi: 10.1016/j.renene.2017.04.035.

[29] Y. Liu, Y. Man, and J. Ren, "Chapter 3 - Waste-to-wealth by sludge-to-energy: a comprehensive literature reviews," in *Waste-to-Energy*, J. Ren, Ed., Academic Press, 2020, pp. 45–74. doi: https://doi.org/10.1016/B978-0-12-816394-8.00003-3.

[30] D. López-González, M. Puig-Gamero, F. G. Acién, F. García-Cuadra, J. L. Valverde, and L. Sanchez-Silva, "Energetic, economic and environmental assessment of the pyrolysis and combustion of microalgae and their oils," Aug. 11, 2015, *Elsevier Ltd*. doi: 10.1016/j.rser.2015.07.022.
[31] S. Tan *et al.*, "Utilization of current pyrolysis technology to convert biomass and manure waste into biochar for soil remediation: A review," Mar. 15, 2023, *Elsevier B.V.* doi: 10.1016/j.scitotenv.2022.160990.
[32] J. Tang, W. Zhu, R. Kookana, and A. Katayama, "Characteristics of biochar and its application in remediation of contaminated soil," *J Biosci Bioeng*, vol. 116, no. 6, pp. 653–659, 2013, doi: 10.1016/j.jbiosc.2013.05.035.
[33] B. Handiso, T. Pääkkönen, and B. P. Wilson, "Effect of pyrolysis temperature on the physical and chemical characteristics of pine wood biochar," *Waste Management Bulletin*, vol. 2, no. 4, pp. 281–287, Dec. 2024, doi: 10.1016/j.wmb.2024.11.008.
[34] P. R. Yaashikaa, P. S. Kumar, S. Varjani, and A. Saravanan, "A critical review on the biochar production techniques, characterization, stability and applications for circular bioeconomy," Dec. 01, 2020, *Elsevier B.V.* doi: 10.1016/j.btre.2020.e00570.
[35] F. Razzaghi, P. B. Obour, and E. Arthur, "Does biochar improve soil water retention? A systematic review and meta-analysis," *Geoderma*, vol. 361, no. September, p. 114055, 2020, doi: 10.1016/j.geoderma.2019.114055.
[36] Y. Zhang, K. Gu, J. Li, C. Tang, Z. Shen, and B. Shi, "Effect of biochar on desiccation cracking characteristics of clayey soils," *Geoderma*, vol. 364, no. August 2019, p. 114182, 2020, doi: 10.1016/j.geoderma.2020.114182.
[37] S. Wijitkosum, T. Sriburi, and P. Toonsiri, "Effect of One-Time Application of Biochar and Compost on Soil and Maize During 5-Time Consecutive Periods of Crop Cultivation," *Emerging Science Journal*, vol. 9, no. 1, pp. 114–130, Feb. 2025, doi: 10.28991/ESJ-2025-09-01-07.
[38] S. Zhao, B. Huang, X. Shu, and P. Ye, "Laboratory investigation of biochar-modified asphalt mixture," *Transp Res Rec*, vol. 2445, pp. 56–63, 2014, doi: 10.3141/2445-07.
[39] S. Zhao, B. Huang, X. P. Ye, X. Shu, and X. Jia, "Utilizing bio-char as a bio-modifier for asphalt cement: A sustainable application of bio-fuel by-product," *Fuel*, vol. 133, pp. 52–62, Oct. 2014, doi: 10.1016/j.fuel.2014.05.002.
[40] W. Dong, F. Ma, C. Li, Z. Fu, Y. Huang, and J. Liu, "Evaluation of Anti-Aging Performance of Biochar Modified Asphalt Binder," *Coating*, vol. 10, no. 11, pp. 1–19, 2020, doi: 10.3390/coatings10111037.
[41] M. Yegane, B. Y. Katanalp, and P. Ahmedzade, "Effects of using biochar materials obtained from cherry and sour cherry wastes on bitumen modification," *Constr Build Mater*, vol. 470, Apr. 2025, doi: 10.1016/j.conbuildmat.2025.140609.
[42] R. Zhang, H. Wang, J. Ji, and H. Wang, "Viscoelastic Properties, Rutting Resistance, and Fatigue Resistance of Waste Wood-Based Biochar-Modified Asphalt," *Coatings*, vol. 12, no. 1, Jan. 2022, doi: 10.3390/coatings12010089.
[43] X. Gan and W. Zhang, "Application of biochar from crop straw in asphalt modification," *PLoS One*, vol. 16, no. 2 February, pp. 1–11, 2021, doi: 10.1371/journal.pone.0247390.
[44] A. Kumar, R. Choudhary, R. Narzari, R. Kataki, and S. K. Shukla, "Evaluation of bio-asphalt binders modified with biochar: a pyrolysis by-product of Mesua ferrea seed cover waste," *Cogent Eng*, vol. 5, no. 1, pp. 1–15, 2018, doi: 10.1080/23311916.2018.1548534.
[45] X. Zhou, T. B. Moghaddam, M. Chen, S. Wu, and S. Adhikari, "Biochar removes volatile organic compounds generated from asphalt," *Science of the Total Environment*, vol. 745, no. 27, p. 141096, 2020, doi: 10.1016/j.scitotenv.2020.141096.
[46] Y. Zhou, C. Shen, T. Wang, and Y. Xue, "Inhibition effect of three types of biochar on volatile organic compounds from asphalt: Revealing chemical adsorption as the primary mechanism," *Constr Build Mater*, vol. 411, Jan. 2024, doi: 10.1016/j.conbuildmat.2023.134322.
[47] A. Allegrini, P. Salvaneschi, B. Schirone, K. Cianfaglione, and A. Di Michele, "Multipurpose plant species and circular economy: Corylus avellana L. as a study case," *Frontiers in Bioscience - Landmark*, vol. 27, no. 1, Jan. 2022, doi: 10.31083/j.fbl2701011.
[48] A. Di Michele *et al.*, "Hazelnut shells as source of active ingredients: Extracts preparation and characterization," *Molecules*, vol. 26, no. 21, Nov. 2021, doi: 10.3390/molecules26216607.

[49] J. Zhao, X. Wang, H. Lin, and Z. Lin, "Hazelnut and its by-products: A comprehensive review of nutrition, phytochemical profile, extraction, bioactivities and applications," Jul. 01, 2023, *Elsevier Ltd*. doi: 10.1016/j.foodchem.2023.135576.
[50] R. Herrera, J. Hemming, A. Smeds, O. Gordobil, S. Willför, and J. Labidi, "Recovery of bioactive compounds from hazelnuts and walnuts shells: Quantitative–qualitative analysis and chromatographic purification," *Biomolecules*, vol. 10, no. 10, pp. 1–16, Oct. 2020, doi: 10.3390/biom10101363.
[51] E. Z. Hoşgün and B. Bozan, "Effect of Different Types of Thermochemical Pretreatment on the Enzymatic Hydrolysis and the Composition of Hazelnut Shells," *Waste Biomass Valorization*, vol. 11, no. 7, pp. 3739–3748, Jul. 2020, doi: 10.1007/s12649-019-00711-z.
[52] FAO, "Agricultural statistical database," Food and Agriculture Organization of the United Nations. Accessed: Apr. 06, 2025. [Online]. Available: http://www.https//www.fao.org/faostat/es/#data/QCL/visualize
[53] C. Martínez-Toledo *et al.*, "Optimising slow pyrolysis parameters to enhance biochar European hazelnut shell as a biobased asphalt modifier," *Materials Today Sustainability*, vol. 30, p. 101087, Jun. 2025, doi: 10.1016/j.mtsust.2025.101087.
[54] F. Ma *et al.*, "Biochar for asphalt modification: A case of high-temperature properties improvement," *Science of the Total Environment*, vol. 804, p. 150194, 2022, doi: 10.1016/j.scitotenv.2021.150194.
[55] AASHTO, "AASHTO T 240: Standard Method of Test for Effect of Heat and Air on a Moving Film of Asphalt Binder (Rolling Thin-Film Oven Test)," 2013.
[56] AASHTO, "AASHTO R 28: Standard Practice for Accelerated Aging of Asphalt Binder Using a Pressurized Aging Vessel (PAV)," 2012.
[57] J. Nahuelcura *et al.*, "Antioxidant Response, Phenolic Compounds and Yield of Solanum tuberosum Tubers Inoculated with Arbuscular Mycorrhizal Fungi and Growing under Water Stress," *Plants*, vol. 12, no. 24, Dec. 2023, doi: 10.3390/plants12244171.
[58] D. Berríos *et al.*, "The Biosynthesis, Accumulation of Phenolic Compounds and Antioxidant Response in Lactuca sativa L. Plants Inoculated with a Biofertilizer Based on Soil Yeast and Iron Nanoparticles," *Plants*, vol. 13, no. 3, Feb. 2024, doi: 10.3390/plants13030388.
[59] R. Jing, A. Varveri, X. Liu, A. Scarpas, and S. Erkens, "Ageing effect on chemo-mechanics of bitumen," *Road Materials and Pavement Design*, vol. 22, no. 5, pp. 1044–1059, 2021, doi: 10.1080/14680629.2019.1661275.
[60] AASHTO, "AASHTO T 316: Standard Method of Test for Viscosity Determination of Asphalt Binder Using Rotational Viscometer," 2019.
[61] ASTM, "ASTM D36-76: Standard Test Method for Softening Point of Bitumen (Ring-and-Ball Apparatus)," 2014, doi: 10.1520/D0036.
[62] ASTM, "Standard Test Method for Penetration of Bituminous Materials," 2013, doi: 10.1520/D0005-13.
[63] R. N. Hunter, *The Shell Bitumen Handbook*, Sixth edit. Shell Bitumen UK, 2014.
[64] AENOR, "UNE-EN 12593-2007: Bitumen and bituminous binders-Determination of the Fraass breaking point," 2007.
[65] AASHTO, "AASHTO T 315: Standard Method of Test for Determining the Rheological Properties of Asphalt Binder Using a Dynamic Shear Rheometer (DSR)," 2020.
[66] A. H. Ali, N. S. Mashaan, and M. R. Karim, "Investigations of physical and rheological properties of aged rubberised bitumen," *Advances in Materials Science and Engineering*, pp. 1–8, 2013, doi: https://doi.org/10.1155/2013/239036.
[67] AASHTO, "AASHTO T 350: Standard Method of Test for Multiple Stress Creep Recovery (MSCR) Test of Asphalt Binder Using a Dynamic Shear Rheometer (DSR)," 2019.
[68] K. Mooney, "Current Status for Multiple Stress Creep Recovery," 2008, *North East Asphalt User / Producer Group Annual Meeting*.
[69] L. G. Loría-Salazar, J. M. Cuadrado-Valbuena, R. E. Villegas-Villegas, and E. A. Castillo-Camarena, "Introducción a los cementos y ligantes asfálticos: caracterización, reología y producción."
[70] R. E. Villegas-Villegas, A. Baldi, J. P. Aguiar-Moya, L. Loria-Salazar, and F. Miranda Arguello, "Relationship between crossover modulus and asphalt chemistry to oxidation process based on

the RHEO+ method," *Road Materials and Pavement Design*, vol. 25, no. sup1, pp. 218–229, 2024, doi: 10.1080/14680629.2023.2203758.
[71] ASTM, "ASTM D7175-15: Standard Test Method for Determining the Rheological Properties of Asphalt Binder Using a Dynamic Shear Rheometer," 2015.
[72] A. Allegrini, P. Salvaneschi, B. Schirone, K. Cianfaglione, and A. Di Michele, "Multipurpose plant species and circular economy: Corylus avellana L. as a study case," *Frontiers in Bioscience - Landmark*, vol. 27, no. 1, pp. 1–20, 2022, doi: 10.31083/j.fbl2701011.
[73] J. Zhao, X. Wang, H. Lin, and Z. Lin, "Hazelnut and its by-products: A comprehensive review of nutrition, phytochemical profile, extraction, bioactivities and applications," *Food Chem*, vol. 413, no. January, p. 135576, 2023, doi: 10.1016/j.foodchem.2023.135576.
[74] A. Di Michele *et al.*, "Hazelnut shells as source of active ingredients: Extracts preparation and characterization," *Molecules*, vol. 26, no. 21, 2021, doi: 10.3390/molecules26216607.
[75] I. Volf, I. Ignat, M. Neamtu, and V. I. Popa, "Thermal stability, antioxidant activity, and photo-oxidation of natural polyphenols," *Chemical Papers*, vol. 68, no. 1, pp. 121–129, Jan. 2014, doi: 10.2478/s11696-013-0417-6.
[76] M. Masullo, A. Cerulli, A. Mari, C. C. de Souza Santos, C. Pizza, and S. Piacente, "LC-MS profiling highlights hazelnut (Nocciola di Giffoni PGI) shells as a byproduct rich in antioxidant phenolics," *Food Research International*, vol. 101, pp. 180–187, Nov. 2017, doi: 10.1016/j.foodres.2017.08.063.
[77] M. L. Greenfield *et al.*, "XANES measurements of sulfur chemistry during asphalt oxidation," *Fuel*, vol. 162, pp. 179–185, Dec. 2015, doi: 10.1016/j.fuel.2015.08.074.
[78] M. Ahmad, M. Khedmati, D. Mensching, B. Hofko, and H. F. Haghshenas, "Aging characterization of asphalt binders through multi-aspect analyses: A critical review," Nov. 15, 2024, *Elsevier Ltd*. doi: 10.1016/j.fuel.2024.132679.
[79] D. Hu, X. Gu, B. Cui, J. Pei, and Q. Zhang, "Modeling the Oxidative Aging Kinetics and Pathways of Asphalt: A ReaxFF Molecular Dynamics Study," *Energy and Fuels*, vol. 34, no. 3, pp. 3601–3613, Mar. 2020, doi: 10.1021/acs.energyfuels.9b03740.
[80] R. C. Walters, E. H. Fini, and Taher. Abu-Lebdeh, "Enhancing Asphalt Rheological Behavior and Aging Susceptibility Using Bio-Char and Nano-Clay," *American Journal of Engineering and Applied Sciences*, vol. 7, no. 1, pp. 66–76, 2014, doi: 10.3844/ajeassp.2014.66.76.
[81] M. E. Çeloglu, M. Yilmaz, K. Baha Vural, and Y. Erkut, "Effects of various biochars on the high temperature performance of bituminous binder," no. June, 2017, doi: 10.14311/ee.2016.232.
[82] C. Martínez-Toledo, G. Valdés-Vidal, A. Calabi-Floody, M. E. González, and O. Reyes-Ortiz, "Effect of Biochar from Oat Hulls on the Physical Properties of Asphalt Binder," *Materials*, vol. 15, no. 19, Oct. 2022, doi: 10.3390/ma15197000.
[83] C. Martinez-Toledo, G. Valdes-Vidal, A. Calabi-Floody, M. E. Gonzalez, and O. Reyes-Ortiz, "Evaluation of Rheological Properties of Asphalt Binder Modified with Biochar from Oat Hulls," *Materials*, vol. 17, no. 17, p. 4312, Aug. 2024, doi: 10.3390/ma17174312.
[84] Y. Liang, J. T. Harvey, D. Jones, and R. Wu, "Evaluation of Age-Hardening on Long-Term Aged Asphalt Binders," *Constr Build Mater*, vol. 304, Oct. 2021, doi: 10.1016/j.conbuildmat.2021.124687.
[85] G. D. Airey, "State of the Art Report on Ageing Test Methods for Bituminous Pavement Materials," Sep. 2003. doi: 10.1080/1029843042000198568.
[86] P. K. Ashish, D. Singh, and S. Bohm, "Investigation on influence of nanoclay addition on rheological performance of asphalt binder," *Road Materials and Pavement Design*, vol. 18, no. 5, pp. 1007–1026, Sep. 2017, doi: 10.1080/14680629.2016.1201522.
[87] G. Xu, H. Wang, and H. Zhu, "Rheological properties and anti-aging performance of asphalt binder modified with wood lignin," *Constr Build Mater*, vol. 151, pp. 801–808, Oct. 2017, doi: 10.1016/j.conbuildmat.2017.06.151.
[88] M. A. Notani *et al.*, "Investigating the high-temperature performance and activation energy of carbon black-modified asphalt binder," *SN Appl Sci*, vol. 2, no. 2, Feb. 2020, doi: 10.1007/s42452-020-2102-z.
[89] AASHTO, "AASHTO M 332: Standard Specification for Performance-Graded Asphalt Binder Using Multiple Stress Creep Recovery (MSCR) Test," 2021.